

1           **A total energy error analysis of dynamical cores and**  
2           **physics-dynamics coupling in the Community Atmosphere**  
3           **Model (CAM)**

4           **Peter H. Lauritzen<sup>1\*</sup>, and David L. Williamson<sup>1</sup>**

5           <sup>1</sup>National Center for Atmospheric Research, Boulder, Colorado, USA

6           **Key Points:**

- 7           • Spurious total energy dissipation in dynamical core is  $-0.3W/m^2$  to  $-1W/m^2$  at 1  
8           degree  
9           • Constant-pressure assumption in physics leads to  $0.3W/m^2$  spurious total energy  
10           source  
11           • There can easily be compensating errors in total energy budget

---

\*1850 Table Mesa Drive, Boulder, Colorado, USA

Corresponding author: Peter Hjort Lauritzen, pel@ucar.edu

12 **Abstract**

13 A closed total energy (TE) budget is of utmost importance in coupled climate system  
 14 modeling; in particular, the dynamical core or physics-dynamics coupling should ideally  
 15 not lead to spurious TE sources/sinks. To assess this in a global climate model, a detailed  
 16 analysis of the spurious sources/sinks of TE in NCAR's Community Atmosphere Model  
 17 (CAM) is given. This includes spurious sources/sinks associated with the parameteriza-  
 18 tion suite, the dynamical core, TE definition discrepancies and physics-dynamics coupling.  
 19 The latter leads to a detailed discussion of the pros and cons of various physics-dynamics  
 20 coupling methods commonly used in climate/weather modeling.

21 **1 Introduction**

22 In coupled climate modeling with prognostic atmosphere, ocean, land, land-ice, and  
 23 sea-ice components, it is important to conserve total energy (TE) to a high degree in each  
 24 component individually and in the complete model to avoid spurious long term trends in  
 25 the simulated Earth system. Conservation of TE in this context refers to having a closed  
 26 TE budget. For example, the TE change in a column in the atmosphere is exactly balanced  
 27 by the net sources/sinks given by the fluxes through the column. The fluxes into the at-  
 28 mospheric component from the surface models must be balanced by the fluxes in the re-  
 29 spective surface components and so on. Henceforth we will focus only on the atmospheric  
 30 component which, in a numerical model, is split into a resolved-scale component (the dy-  
 31 namical core) and a sub-grid-scale component (parameterizations or, in modeling jargon,  
 32 physics). While there have been many studies on energy flow in the Earth system through  
 33 analysis of re-analysis data and observations [Trenberth and Fasullo, 2018, and references  
 34 therein], there has been less focus on spurious TE sources/sinks in numerical models.

35 The atmospheric equations of motion conserve TE but the discretizations used in cli-  
 36 mate and weather models are usually not inherently TE conservative. Exact conservation  
 37 is probably not necessary but conservation to within  $\sim 0.01 \text{ W/m}^2$  has been considered  
 38 sufficient to avoid spurious trends in century long simulations [Boville, 2000; Williamson  
 39 *et al.*, 2015]. Spurious sources and sinks of TE can be introduced by the dynamical core,  
 40 physics, physics-dynamics coupling as well as discrepancies between the TE of the con-  
 41 tinuous and discrete equations of motion and for the physics. Hence the study of TE con-  
 42 servation in comprehensive models of the atmosphere quickly becomes a quite complex  
 43 and detailed matter. In addition there can easily be compensating errors in the system as a  
 44 whole.

45 Here we focus on versions of the Community Atmosphere Model (CAM) that use  
 46 the spectral-element [SE, Lauritzen *et al.*, 2018] and finite-volume [FV, Lin, 2004] dy-  
 47 namical cores. These dynamical cores couple with physics in a time-split manner, i.e.  
 48 physics receives a state updated by dynamics [see Williamson, 2002, for a discussion  
 49 of time-split versus process split physics-dynamics coupling in the context of CAM]. In  
 50 its pure time-split form the physics tendencies are added to the state previously produced  
 51 by the dynamical core and the resulting state provides the initial state for the subsequent  
 52 dynamical core calculation. We refer to this as *state-updating* (`ftype=1` in CAM code).  
 53 Alternatively, when the dynamical core adopts a shorter time step than the physics, say  
 54 `nsplit` sub-steps, then  $(1/\text{nsplit})$ th of the physics-calculated tendency is added to the  
 55 state before each dynamics sub-step. We refer to this modification of time-splitting as  
 56 *dribbling* (`ftype=0`). CAM-FV uses the *state-update* (`ftype=1`) approach while CAM-SE  
 57 has options to use *state-update* (`ftype=1`), *dribbling* (`ftype=0`) or a combination of the  
 58 two i.e. mass-variables use *state-updating* and remaining variables use *dribbling*. We refer  
 59 to this as *combination* (`ftype=2`). The *dribbling* variants can lead to spurious sources or  
 60 sinks of TE (and mass) referred to here as physics-dynamics coupling errors. Any error  
 61 in the water mass-budget associated with *dribbling* affects the mass-weightening in the TE  
 62 integral and hence introduces TE errors.

The dynamical core usually has inherent or specified filters to control spurious noise near the grid scale which will lead to energy dissipation [Thuburn, 2008; Jablonowski and Williamson, 2011]. Similarly models often have sponge layers to control the solution near the top of the model that may be a sink of TE. There are examples of numerical discretizations of the adiabatic frictionless equations motion that are designed so that TE is conserved in the absence of time-truncation and filtering errors, e.g., mimetic spectral-element discretizations such as the one used in the horizontal in CAM-SE [Taylor, 2011; Eldred and Randall, 2017; McRae and Cotter, 2013]. These provide consistency between the discrete momentum and thermodynamic equations leading to global conservation associated with the conversion of potential to kinetic energy. In spectral transform models it is customary to add the energy change due to explicit diffusion on momentum back as heating (referred to as frictional heating), so that the diffusion of momentum does not affect the TE budget [see, e.g., p.71 in Neale *et al.*, 2012]. This is also done in CAM-SE [Lauritzen *et al.*, 2018].

The purpose of this paper is to provide a detailed global TE analysis of CAM. We assess TE errors due to various steps in the model algorithms. The paper is outlined as follows. In section 2 the continuous TE formulas are given and a detailed description of spurious TE sources/sinks that can occur in a model as a whole, and the associated diagnostics used to perform the TE analysis, are defined. In section 3 the model is run in various configurations to assess their effects on TE conservation. This includes various physics-dynamics coupling experiments leading to a rather detailed discussion of mass budget closure. We also investigate the effect of using a limiter in the vertical remapping of momentum, assess energy discrepancy errors and impacts on TE of simplifying surface conditions and dry atmosphere experiments. The paper ends with conclusions.

## 2 Method

### 2.1 Defining total energy (TE)

In the following it is assumed that the model top and bottom are coordinate surfaces and that there is no flux of mass through the model top and bottom. In a dry hydrostatic atmosphere the TE equation integrated over the entire sphere is given by

$$\frac{d}{dt} \int_{z=z_s}^{z=z_{top}} \iint_S E_v \rho^{(d)} dA dz = \int_{z=z_s}^{z=z_{top}} \iint_S F_{net} \rho^{(d)} dA dz, \quad (1)$$

[e.g., Kasahara, 1974] where  $F_{net}$  is net flux calculated by the parameterizations (e.g., heating and momentum forcing),  $d/dt$  the total/material derivative,  $z_s$  is the height of the surface,  $S$  the sphere,  $\rho^{(d)}$  the density of dry air,  $E_v$  is the TE and  $dA$  is an infinitesimal area on the sphere.  $E_v$  can be split into kinetic energy  $K = \frac{1}{2}\mathbf{v}^2$  ( $\mathbf{v}$  is the wind vector), internal energy  $c_v^{(d)}T$ , where  $c_v^{(d)}$  is the heat capacity of dry air at constant volume, and potential energy  $\Phi = gz$

$$E_v = K + c_v^{(d)}T + \Phi. \quad (2)$$

If the vertical integral is performed in a mass-based vertical coordinate, e.g., pressure, then the integrated TE equation for a dry atmosphere can be written as

$$\frac{d}{dt} \int_{p=p_s}^{p=p_{top}} \iint_S E_p dA dp + \frac{d}{dt} \iint_S \Phi_s p_s dA = \int_{p=p_s}^{p=p_{top}} \iint_S F_{net} dA dp, \quad (3)$$

[e.g., Kasahara, 1974] where

$$E_p = K + c_p^{(d)}T. \quad (4)$$

In a moist atmosphere, however, there are several definitions of TE used in the literature related to what heat capacity is used for water vapor and whether or not condensates are accounted for in the energy equation. To explain the details of that we focus on the energy equation for CAM-SE.

CAM-SE is formulated using a terrain-following hybrid-sigma vertical coordinate  $\eta$  but the coordinate levels are defined in terms of dry air mass per unit area ( $M^{(d)}$ ) instead of total air mass;  $\eta^{(d)}$  [see *Lauritzen et al.*, 2018, for details]. In such a coordinate system it is convenient to define the tracer state in terms of a dry mixing ratio instead of moist mixing ratio

$$m^{(\ell)} \equiv \frac{\rho^{(\ell)}}{\rho^{(d)}}, \text{ where } \ell = \{'wv', 'cl', 'ci', 'rn', 'sw'\}, \quad (5)$$

where  $\rho^{(d)}$  is the mass of dry air per unit volume of moist air and  $\rho^{(\ell)}$  is the mass of the water substance of type  $\ell$  per unit volume of moist air. Moist air refers to air containing dry air (' $d$ '), water vapor (' $wv$ '), cloud liquid (' $cl$ '), cloud ice (' $ci$ '), rain amount (' $rn$ ') and snow amount (' $sw$ '). For notational purposes define the set of all components of air

$$\mathcal{L}_{all} = \{'d', 'wv', 'cl', 'ci', 'rn', 'sw'\}, \quad (6)$$

Define associated heat capacities at constant pressure  $c_p^{(\ell)}$ . We refer to condensates as being *thermodynamically and inertially active* if they are included in the thermodynamic equation and momentum equations; e.g. if the thermodynamic equation is formulated in terms of temperature, the energy conversion term includes a generalized heat capacity which is a function of the condensates and their associated heat capacities [see, e.g., section 2.3 in *Lauritzen et al.*, 2018]. Similarly the weight of the condensates is included in the pressure field and pressure gradient force. How many and which condensates are thermodynamically/inertially active in the dynamical core is controlled with namelist `qsize_condensate_loading`. If `qsize_condensate_loading=1` only water vapor (' $wv$ ') is active, `qsize_condensate_loading=3` ' $wv$ ', ' $cl$ ', and ' $ci$ ' are active, and if `qsize_condensate_loading=5` then ' $wv$ ', ' $cl$ ', ' $ci$ ', ' $rn$ ', and ' $sw$ ' are included.

Using the  $\eta^{(d)}$  vertical coordinate and dry mixing ratios the TE (per unit area) that the frictionless adiabatic equations of motion in the CAM-SE dynamical core conserves is

$$\widehat{E}_{dyn} = \frac{1}{\Delta S} \int_{\eta=0}^{\eta=1} \iint_S \left( \frac{1}{g} \frac{\partial M^{(d)}}{\partial \eta^{(d)}} \right) \sum_{\ell \in \mathcal{L}_{all}} \left[ m^{(\ell)} \left( K + c_p^{(\ell)} T + \Phi_s \right) \right] dA d\eta^{(d)}, \quad (7)$$

where  $\Delta S$  is the surface area of the sphere,  $\Phi_s$  is the surface geopotential and  $\widehat{(\cdot)}$  refers to the global average.

In the CAM physical parameterizations a different definition of TE is used. Due to the evolutionary nature of the model development, the parameterizations have not yet been converted to match the SE dynamical core. For the computation of TE, condensates are assumed to be zero and the heat capacity of moisture is the same as for dry air. This is equivalent to using a moist mass (dry air plus water vapor) but  $c_p$  of dry air:

$$\widehat{E}_{phys} = \frac{1}{\Delta S} \int_{\eta=0}^{\eta=1} \iint_S \left( \frac{1}{g} \frac{\partial M^{(d)}}{\partial \eta^{(d)}} \right) \left( 1 + m^{(wv)} \right) \left[ \left( K + c_p^{(d)} T + \Phi_s \right) \right] dA d\eta^{(d)}. \quad (8)$$

We note that earlier versions of CAM using the spectral transform dynamical core used  $c_p$  of moist air. The adiabatic, frictionless equations of motion in the CAM-SE dynamical core can be made consistent with  $E_{phys}$  by not including condensates in the mass/pressure field as well as energy conversion term in the thermodynamic equation and setting the heat capacity for moisture to  $c_p^{(d)}$  [Taylor, 2011]. We refer to this version of CAM-SE combined with *state-updating* (`ftype=1`) physics-dynamics coupling as the *energy consistent* version; i.e. the same continuous formula for energy is used in both dynamics and physics, and there are no physics-dynamics coupling errors.

## 2.2 Some remarks on local energy conservation

Although this paper focuses on global average TE errors, it is important to note that energy errors occur locally. For example, when an air parcel gains or loses water via

145 evaporation or precipitation (or via a fixer or borrower to maintain some physical property  
 146 like positive definiteness), there are implications for the mass, heat content, and heat ca-  
 147 pacity of the parcel. In turn, that affects the energy and mass of the column and thereby  
 148 affects the global TE budget. So anything that changes these state variables locally has  
 149 implications for the TE budget.

150 An example of an inconsistency in CAM physics is that surface pressure is held  
 151 fixed during physical parameterization updates but water vapor, and hence surface pres-  
 152 sure, does change during evaporation/precipitation and an inconsistency appears in the  
 153 mass and energy budget (see item 2 in Section 2.3). Similarly, if a ‘clipper’ is used on  
 154 water vapor or condensates to avoid (unphysical) negative mixing ratios (more details in  
 155 section 3.2) and this is not accounted for in the thermodynamics or through a surface flux,  
 156 that ‘clipping’ will produce an energy source via the mass-weightening in the TE vertical  
 157 integral. In the dynamical core TE is not conserved locally in each column as there is a  
 158 horizontal flux of energy between columns; but the local energy budget should, ideally, be  
 159 closed and thereby globally TE should be conserved. If a dynamical core does not inher-  
 160 ently conserve dry air mass and/or water mass then a spurious source of TE is inevitable  
 161 again through the mass-weightening in the vertical integral (unless fixers are applied).

### 162 2.3 Spurious energy sources and sinks

163 In a weather/climate model TE conservation errors can appear in many places through-  
 164 out the algorithm. Below is a general list of where conservation errors can appear with  
 165 specific examples from CAM:

- 166 1. *Parameterization errors*: Individual parameterizations may not have a closed energy  
     167 budget ; for example, they may not have been designed to conserve the discrete  
     168 TE as defined in the model or they may conserve a discrete TE defined differently.  
     169 CAM parameterizations are required to have a closed energy budget (based on the  
     170 discrete TE definition in CAM) under the assumption that pressure remains con-  
     171 stant during the computation of the subgrid-scale parameterization tendencies. In  
     172 other words, the TE change in the column is exactly balanced by the net sources/sinks  
     173 given by the fluxes through the column<sup>1</sup>.
- 174 2. *Pressure work error*: That said, if parameterizations update specific humidity then  
     175 the surface pressure changes (e.g., moisture entering or leaving the column). In  
     176 that case the pressure changes which, in turn, changes TE. This is referred to as  
     177 *pressure work error* [section 3.1.8 in *Neale et al.*, 2012].
- 178 3. *Continuous TE formula discrepancy*: If the continuous equations of motion for the  
     179 dynamical core conserve a TE different from the one used in the parameterizations  
     180 then an energy inconsistency is present in the system as a whole. This is the case  
     181 with the new version of CAM-SE that conserves a TE that is more accurate and  
     182 comprehensive than that used in the CAM physics package as discussed above. As  
     183 also noted above, this mismatch arose from the evolutionary nature of the model  
     184 development and not by deliberate design; and should be eliminated in the future.
- 185 4. *Dynamical core errors*: Energy conservation errors in the dynamical core, not re-  
     186 lated to physics-dynamics coupling errors, can arise in multiple parts of the algo-  
     187 rithms used to solve the equations of motion. For dynamical cores employing fil-  
     188 tering [e.g., limiters in flux operators *Lin*, 2004] and/or possessing inherent damp-  
     189 ing which controls small scales, it is hard to isolate their energy dissipation from  
     190 other errors in the discretization. If a hyperviscosity term or some other diffusion  
     191 is added to the momentum equation, then one can diagnose the local energy diss-

---

<sup>1</sup> If not, a fixer needs to be applied since the CAM global TE fixer as implemented does not include any errors from the parameterizations. For example, in CAM parameterizations occasionally produce negative water vapor. These are filled without compensation and therefore affect the TE but errors tend to be small.

192 pation from such damping and add a corresponding heating to balance it (frictional  
 193 heating). There may also be energy loss from viscosity applied to other variables  
 194 such a temperature or pressure which is harder to compensate. Here is a break-down  
 195 relevant to CAM-SE using a floating Lagrangian vertical coordinate:

- 196 • Horizontal inviscid dynamics: Energy errors resulting from solving the inviscid,  
 197 adiabatic equations of motion.
- 198 • Hyperviscosity: Filtering errors.
- 199 • Vertical remapping: The vertical remapping algorithm from Lagrangian to Eule-  
 200 rian reference surfaces does not conserve TE.
- 201 • Near round-off negative values of water vapor which are filled to a minimal  
 202 value without compensation.

203 If a dynamical core is not inherently mass-conservative with respect to dry air, wa-  
 204 ter vapor and condensates then TE conservation is affected since

$$\int_{\eta=0}^{\eta=1} \iint_S \left( \frac{1}{g} \frac{\partial M^{(d)}}{\partial \eta^{(d)}} \right) \sum_{\ell \in \mathcal{L}_{all}} [m^{(\ell)}] dA d\eta^{(d)} \quad (9)$$

205 is not conserved. Henceforth we assume that the dynamical core is based on an  
 206 inherently mass-conservative formulation which is the case for CAM-SE, CAM-SE-  
 207 CSLAM and CAM-FV.

- 208 5. *Physics-dynamics coupling (PDC)*: Assume that physics computes a tendency. Usu-  
 209 ally the tendency (forcing) is passed to the dynamical core which is responsible for  
 210 adding the tendencies to the state. PDC energy errors can be split into three types:

- 211 • ‘Dribbling’ errors (or, equivalently, temporal PDC errors): If the TE increment  
 212 from the parameterizations does not match the change in TE when the tenden-  
 213 cies are added to the state in the dynamical core, then there will be a spurious  
 214 PDC error. This will not happen with the *state-update* approach in which the  
 215 tendencies are added immediately after physics and before the dynamical core  
 216 advances the solution in time. The PDC ‘dribbling’ errors can be split into 3  
 217 contributions:

218 *Thermal energy ‘dribbling’ error*: PDC errors in temperature tendencies occur  
 219 because the  $T$ -increment (call it  $\Delta T$ ) that the parameterizations prescribe leads  
 220 to a dry thermal energy change of  $\Delta M^{(d)} \Delta T$  which will not match the equivalent  
 221 dry thermal energy change when the temperature tendency is added in smaller  
 222 chunks in the dynamical core during the ‘dribbling’ of  $\Delta T$ . The discrepancy  
 223 occurs because  $\Delta M^{(d)}$  changes during each dynamics time-step and hence the  
 224 thermal energy change due to physics forcing accumulated during the ‘dribbling’  
 225 will not equal  $\Delta M^{(d)} \Delta T$ . This error could possibly be eliminated by using ther-  
 226 mal energy forcing instead of temperature increments.

227 *Kinetic energy ‘dribbling’ error*: Similarly, PDC errors in velocity component  
 228 forcing increments ( $\Delta u, \Delta v$ ) occur because the dry kinetic energy change of  $\Delta M^{(d)} [(\Delta u)^2 + (\Delta v)^2]$   
 229 will not match the equivalent dry kinetic energy change when ‘dribbling’ veloc-  
 230 ity component forcing increments ( $\Delta u, \Delta v$ ). It is less clear how to eliminate this  
 231 error as kinetic energy is a quadratic quantity.

232 *Mass ‘clipping’ (affects all TE terms)*: A similar PDC error for mass-variables  
 233 such as vapor vapor forcing, cloud liquid, etc. can occur when the mass-tendencies  
 234 are ‘dribbled’ during the dynamical core integration. The dynamical core trans-  
 235 port of mass variables will move mass around in the horizontal and vertical while  
 236 the ‘dribbled’ physics mass increments are applied in the same location; in that  
 237 situation a negative mass-increment from the parameterizations may be larger  
 238 than the mass available to remove. This can lead to a spurious source mass if  
 239 there is logic in the dynamical core preventing mixing ratios/mass to become  
 240 negative. This is referred to as ‘clipping’ PDC errors and the process is de-  
 241 scribed/discussed in detail in Section 3.2.1. The ‘clipping’ changes the water

mass budget without accounting for it in water fluxes or in the thermodynamics and hence lead to a TE conservation errors (both kinetic and thermal energy).

- *Change of vertical grid/coordinate errors:* If the vertical coordinates in physics and in the dynamical core are different then there can be spurious PDC energy errors even when using the state-update method for adding tendencies to the dynamical core state. For example, many non-hydrostatic dynamical cores [e.g. Skamarock *et al.*, 2012] use a terrain-following height coordinate whereas physics uses pressure.
- *Change of horizontal grid errors:* If the physics tendencies are computed on a different horizontal grid than the dynamical core then there can be spurious energy errors from mapping tendencies and/or variables between horizontal grids [e.g., Herrington *et al.*, 2018].

6. *Compensating Energy fixers:* To avoid TE conservation errors which could accumulate and ultimately lead to a climate drift, it is customary to apply an arbitrary energy fixer to restore TE conservation. Since the spatial distribution of many energy errors, in general, is not known, global fixers are used. In CAM a uniform increment is added to the temperature field to compensate for TE imbalance from all processes, i.e. dynamical core, physics-dynamics coupling, TE formula discrepancy, and energy change due to pressure work error.

## 2.4 Diagnostics

The discrete global averages ( $\widehat{\cdot}$ ) are computed consistent with the discrete model grid as outlined in section 2.2. of Lauritzen *et al.* [2014]. The TE global average tendency is denoted

$$\partial \widehat{E} \equiv \frac{d\widehat{E}}{dt}. \quad (10)$$

By computing the global TE averages  $\widehat{E}$  at appropriate places in the model algorithms, we can directly compute  $\partial \widehat{E}$  due to various processes (such as viscosity, vertical remapping, physics-dynamics coupling, pressure work error, etc.) by differencing  $\widehat{E}$  from after and before the algorithm takes place. This has been implemented using CAM history infrastructure by computing column integrals of energy at various places in CAM and outputting the 2D energy fields. CAM history internally handles accumulation and averaging in time at each horizontal grid point. The global averages are computed externally from the grid point vertical integrals on the history files (stored in double precision). The places in CAM where we compute/capture the grid point vertical integral  $E$  are named using three letters where the first letter refers to whether the vertical integral is performed in physics ('p') or in the dynamical core ('d'). The trailing two letters refer to the specific location in dynamics or physics. For example, 'BP' refers to 'Before Physics' and 'AP' to 'After Physics'; the associated total energies are denoted  $E_{pBP}$  and  $E_{pAP}$ , respectively. The TE tendency from the parameterizations is the difference between  $E_{pBP}$  and  $E_{pAP}$  divided by the time-step. The terms and tendencies are then averaged globally externally to the model. The pseudo-code in Figure 1 defines the acronyms in terms of where in the CAM-SE algorithm the TE vertical integrals are computed and output. For details on the CAM-SE algorithm please see Lauritzen *et al.* [2018].

Before defining the individual terms in detail we briefly review the model time stepping sequence starting with the physics component as illustrated in Figure 1. The energy fixer is applied first to compensate for the spurious net energy change from all components introduced during the previous time step. We will describe this in more detail after the various sources and sinks are elucidated. The parameterizations are applied next and are required to be energy conserving. They update the state and accumulate the total physics tendency (forcing). At this stage the state is saved for use in the energy fixer in the next time step. Any changes in the global average energy after this are spurious and are compensated by the fixer. The parameterizations update the water vapor but not the

moist pressure, implying a non-physical change in the dry mass of the atmosphere. The dry mass correction corrects the dry mass back to its proper value.

The forcing (physics tendency) from the parameterizations is passed to the dynamical core. If the physics and dynamics operate on different grids, the forcing is remapped here. The dynamics operates on a shorter time step than the physics and is sub-stepped. The remapped physics increment is applied to the dynamics state, saved from the end of the previous dynamics step, using either *state-updating*, *dribbling*, or *combination* as described in the introduction. The dynamics then advances the adiabatic frictionless flow in the floating Lagrangian layers over a further set of sub-steps. Hyperviscosity is applied next with further sub-stepping required for computational stability of the explicit discrete approximations. The energy loss from the specified momentum viscosity is calculated locally and is balanced by adding a local change to the temperature, referred to as *frictional heating*. This set of dynamics sub-steps is followed by the vertical remapping from Lagrangian to Eulerian reference layers. The remapping is required to provide layers consistent with the parameterization formulations. The vertical remapping sub-steps are required for stability if the Lagrangian layers become too thin.

At the end of the dynamics, the state is saved to be used by the dynamics the next time step and is also passed to the physics, with a remapping if the dynamics and physics grids differ. At the beginning of the physics the difference in energy between this state and the state saved after the physics during the previous time step is the amount needed to be added or subtracted by the energy fixer. It represents the accumulation of all spurious sources from the dry mass correction, remappings between physics and dynamics grids (if applicable), dynamical core, differing energy definitions (if present), hyperviscosity, and vertical remapping.

We now define the following energy tendencies corresponding to the itemized list in section 2.3 with references to terms indicated in Figure 1. We start just after the energy fixer which will be defined at the end.

- 324 1.  $\partial \widehat{E}^{(param)}$ : TE tendency due to parameterizations. In CAM the TE budget for each  
 325 parameterization is closed (assuming pressure is unchanged) so  $\partial \widehat{E}^{(param)}$  is bal-  
 326 anced by net fluxes in/out of the physics columns. Note that this is the only energy  
 327 tendency that is not spurious since CAM parameterizations have a closed TE bud-  
 328 get. This TE tendency is discretely computed as

$$\partial \widehat{E}_{phys}^{(param)} = \frac{\widehat{E}_{pAP} - \widehat{E}_{pBP}}{\Delta t_{phys}}, \quad (11)$$

332 where  $\Delta t_{phys}$  is the physics time-step (default 1800s) and the subscript *phys* on  $\partial \widehat{E}$   
 333 refers to the energy tendency computed in CAM physics. We include the tendency  
 334 to provide a reference scaling for other errors.

- 335 2.  $\partial \widehat{E}^{(pwork)}$ : Total spurious energy tendency due to pressure work error

$$\partial \widehat{E}_{phys}^{(pwork)} = \frac{\widehat{E}_{pAM} - \widehat{E}_{pAP}}{\Delta t_{phys}}. \quad (12)$$

336 Since CAM-SE dynamical core is based on a dry-mass vertical coordinate the pres-  
 337 sure work error takes place implicitly in the dynamical core. But the TE tendency  
 338 due to pressure work error is conveniently computed in physics since dynamical  
 339 cores based on a moist vertical coordinate (e.g., CAM-FV) require pressure and  
 340 moist mixing ratios to be adjusted for dry mass conservation and tracer mass con-  
 341 servation [section 3.1.8 in *Neale et al.*, 2012]. The difference of TE after and be-  
 342 fore this adjustment is the TE tendency due to pressure work error. In a dry mass  
 343 vertical coordinate based on dry mixing ratios neither dry mass layer thickness nor  
 344 dry mixing ratios need to be adjusted to take into account moisture changes in the

345 column. For labeling purposes, the 'total forcing' associated with physics (at least  
 346 in CAM) consists of parameterizations, pressure work error and TE fixer, although  
 347 strictly speaking the fixer includes components from the dynamics as will be seen.

$$\partial \widehat{E}_{phys}^{(phys)} \equiv \partial \widehat{E}_{phys}^{(param)} + \partial \widehat{E}_{phys}^{(pwork)} + \partial \widehat{E}_{phys}^{(efix)} = \frac{\widehat{E}_{pAM} - \widehat{E}_{pBF}}{\Delta t_{phys}}. \quad (13)$$

348 where the energy fixer TE tendency is

$$\partial \widehat{E}_{phys}^{(efix)} = \frac{\widehat{E}_{pBP} - \widehat{E}_{pBF}}{\Delta t_{phys}}. \quad (14)$$

349 After all the TE budget terms have been defined, the exact composition of  $\partial \widehat{E}_{phys}^{(efix)}$   
 350 will be presented.

- 351 3.  $\partial \widehat{E}^{(discr)}$ : If the physics uses a TE definition different from the TE that the con-  
 352 tinuous equations of motion in the dynamical core conserve (i.e. in the absence of  
 353 discretization errors), then there is a TE discrepancy tendency. This complicates  
 354 the energy analysis as one can not compare TE computed in physics  $\widehat{E}_{phys}$  directly  
 355 with TE computed in the dynamical core  $\widehat{E}_{dyn}$ . This makes errors associated with  
 356 this discrepancy tricky to assess. That said, the TE tendencies computed using the  
 357 dynamical core TE formula  $\partial \widehat{E}_{dyn}$  are well defined (self consistent) and similarly  
 358 for TE tendencies computed using the 'physics formula' for TE,  $\partial \widehat{E}_{phys}$ .
- 359 4. The TE tendency from the dynamical core is split into several terms: Horizontal  
 360 adiabatic dynamics (dynamics excluding physics forcing tendency)

$$\partial \widehat{E}_{dyn}^{(2D)} = \frac{\widehat{E}_{dAD} - \widehat{E}_{dBd}}{\Delta t_{dyn}}, \quad (15)$$

361 where over a single dynamics sub-step  $\Delta t_{dyn} = \frac{\Delta t_{phys}}{\text{nsplit} \times \text{rsplit}}$  (the loop bounds  
 362 `nsplit`, `rsplit`, etc. are explained in Figure 1).

363 In CAM-SE the viscosity is explicit so one can compute the TE tendency due to  
 364 hyperviscosity and its associated frictional heating

$$\partial \widehat{E}_{dyn}^{(hvis)} = \frac{\widehat{E}_{dAH} - \widehat{E}_{dBH}}{\Delta t_{hvis}}, \quad (16)$$

365 which, in CAM-SE, includes a frictional heating term from viscosity on momentum

$$\partial \widehat{E}_{dyn}^{(fheat)} = \frac{\widehat{E}_{dAH} - \widehat{E}_{dCH}}{\Delta t_{hvis}}, \quad (17)$$

366 where  $\Delta t_{hvis} = \frac{\Delta t_{phys}}{\text{nsplit} \times \text{rsplit} \times \text{hypervis_subcycle}}$  is the time step of the sub-stepped  
 367 viscosity. Since the viscosity on momentum is compensated for via heating (fric-  
 368 tional heating)  $\partial \widehat{E}_{dyn}^{(hvis)}$  'only' has contributions from viscosity on temperature and  
 369 pressure-level thickness. In terms of TE conservation it would be beneficial if hy-  
 370 perviscosity on temperature and mass could be avoided. However, the hyperviscos-  
 371 ity on mass and temperature is necessary to keep this model stable.

372 The residual

$$\partial \widehat{E}_{dyn}^{(res)} = \partial \widehat{E}_{dyn}^{(2D)} - \partial \widehat{E}_{dyn}^{(hvis)}, \quad (18)$$

373 is the energy error due to inviscid dynamics and time-truncation errors.

374 The energy tendency due to vertical remapping is

$$\partial \widehat{E}_{dyn}^{(remap)} = \frac{\widehat{E}_{dAR} - \widehat{E}_{dAD}}{\Delta t_{remap}}, \quad (19)$$

375 where  $\Delta t_{remap} = \frac{\Delta t_{phys}}{\text{nsplit}}$ .

376 The 3D adiabatic dynamical core (no physics forcing but including friction) energy  
 377 tendency is denoted

$$\partial \widehat{E}_{dyn}^{(adiab)} = \partial \widehat{E}_{dyn}^{(2D)} + \partial \widehat{E}_{dyn}^{(remap)}. \quad (20)$$

378 5.  $\partial \widehat{E}^{(pdc)}$ : Total spurious energy tendency due to physics-dynamics coupling errors is  
 379 the difference between the energy tendency from physics and the energy tendency  
 380 in the dynamics resulting from adding the physics increment to the dynamical core  
 381 state

$$\partial \widehat{E}^{(pdc)} = \partial \widehat{E}_{phys}^{(phys)} - \partial \widehat{E}_{dyn}^{(phys)} \text{ assuming } \partial \widehat{E}^{(discr)} = 0, \quad (21)$$

382 where

$$\partial \widehat{E}_{dyn}^{(phys)} = \frac{\widehat{E}_{dBD} - \widehat{E}_{dAF}}{\Delta t_{pdc}}, \quad (22)$$

383 and  $\Delta t_{pdc}$  is the time-step between physics increments being added to the dynamical  
 384 core. Remember we are dealing with average rates so terms computed with dif-  
 385 ferent time steps can be compared, but differences cannot be taken between terms  
 386 sampled with different time steps.

387 The physics-dynamics coupling TE tendency  $\partial \widehat{E}^{(pdc)}$  makes use of TE formulas  
 388 in dynamics and in physics so (21) is only well-defined if the TE formula discrep-  
 389 ance is zero,  $\partial \widehat{E}^{(discr)} = 0$ . As mentioned in Section 2.1, CAM-SE has the op-  
 390 tion to switch the continuous equations of motion conserving the TE used by CAM  
 391 physics (8) instead of the more comprehensive TE formula (7).

392 In CAM-SE there are 3 physics-dynamics coupling algorithms described in detail  
 393 in section 3.6 in *Lauritzen et al. [2018]* and reviewed in the introduction here. One  
 394 is *state-update* in which the entire physics increments are added to the dynamics  
 395 state at the beginning of dynamics (referred to as `ftype=1`), in which case  $\Delta t_{pdc} =$   
 396  $\Delta t_{phys}$ . Another is *dribbling* in which the physics tendency is split into `nsplit`  
 397 equal chunks and added throughout dynamics (more precisely after every vertical  
 398 remapping; referred to as `ftype=0` resulting in  $\Delta t_{pdc} = \frac{1}{n\text{split}} \Delta t_{phys}$ ), and then a  
 399 *combination* of the two (referred to as `ftype=2`) where tracers (mass variables) use  
 400 *state-update* (`ftype=1`) and all other physics tendencies use *dribbling* (`ftype=0`).

401 6.  $\partial \widehat{E}^{(efix)}$ : Global energy fixer tendency, defined in (14), is applied at the beginning  
 402 of the parameterizations. The correction needed is the global average difference  
 403 between the state passed from the dynamics and the state that was saved after the  
 404 physics updated the state but before the dry mass correction. It includes all spu-  
 405 rious sources from the dry mass correction, remappings between physics and dy-  
 406 namics, dynamical core, differing energy definitions (if present), hyperviscosity, and  
 407 vertical remapping.

## 408 2.5 A few observations regarding the energy budget terms

409 It is useful to note that the energy fixer ‘fixes’ energy errors for the dynamical core,  
 410 pressure work error, physics-dynamics coupling and TE discrepancy

$$-\partial \widehat{E}_{phys}^{(efix)} = \partial \widehat{E}_{phys}^{(pwork)} + \partial \widehat{E}_{dyn}^{(adiab)} + \partial \widehat{E}^{(pdc)} + \partial \widehat{E}^{(discr)}. \quad (23)$$

411 The forcing from the parameterizations,  $\partial \widehat{E}_{phys}^{(param)}$ , does not appear in this budget (al-  
 412 though the dynamical core state does ‘feel’ the parameterization forcing) as the energy  
 413 cycle for the parameterizations is, by design in CAM, closed (balanced by fluxes in/out of  
 414 the physics columns). If  $\partial \widehat{E}^{(discr)} = 0$ , one can use (23) to diagnose energy dissipation  
 415 in the dynamical core and physics-dynamics coupling from quantities computed only in  
 416 physics

$$\partial \widehat{E}_{dyn}^{(adiab)} + \partial \widehat{E}^{(pdc)} = -\partial \widehat{E}_{phys}^{(efix)} - \partial \widehat{E}_{phys}^{(pwork)} \text{ for } \partial \widehat{E}^{(discr)} = 0. \quad (24)$$

417 This is useful if the diagnostics are not implemented in the dynamical core; in particular,  
 418 if the *state-update* (`ftype=1`) physics-dynamics coupling method is used then  $\partial \widehat{E}^{(pdc)} = 0$

419 and the TE errors in the dynamical core can be computed without diagnostics imple-  
 420 mented in the dynamical core. Also, (24) provides an alternative formula for  $\partial\widehat{E}^{(pdc)}$   
 421 compared to (21):

$$\partial\widehat{E}^{(pdc)} = -\partial\widehat{E}_{phys}^{(efix)} - \partial\widehat{E}_{phys}^{(pwork)} - \partial\widehat{E}_{dyn}^{(adiab)} \text{ assuming } \partial\widehat{E}^{(discr)} = 0. \quad (25)$$

422 If  $\partial\widehat{E}^{(pdc)} = 0$  (23) can be used to compute  $\partial\widehat{E}^{(discr)}$

$$\partial\widehat{E}^{(discr)} = -\partial\widehat{E}_{phys}^{(efix)} - \partial\widehat{E}_{phys}^{(pwork)} - \partial\widehat{E}_{dyn}^{(adiab)}, \text{ assuming } \partial\widehat{E}^{(pdc)} = 0. \quad (26)$$

423 Note that we can not use (21) to compute  $\partial\widehat{E}^{(discr)}$  since  $\widehat{E}_{phys} \neq \widehat{E}_{dyn}$ .

### 424 3 Results

425 A series of simulations have been performed with CESM2.1 using CAM version 6  
 426 (CAM6) physics (<https://doi.org/10.5065/D67H1H0V>) on NCAR's Cheyenne cluster  
 427 [*Computational and Information Systems Laboratory*, 2017]. All simulations are at nomi-  
 428 nally  $\sim 1^\circ$  horizontal resolution (for CAM-SE that is  $30 \times 30$  elements on each cubed-  
 429 sphere face and for CAM-FV its  $192 \times 288$  latitudes-longitudes) and using the standard  
 430 32 levels in the vertical. Unless otherwise noted all simulations are 13 months in dura-  
 431 tion and the last 12 months are used in the analysis. Total energy budgets are summarized  
 432 in Table 1 and discussed below. The first column gives identifying 'Descriptors' which  
 433 are briefly summarized below and defined in more detail in the following sections. The  
 434 section titles also include the 'Descriptor' from Table 1 to make it easier for the reader  
 435 to match Table entries with discussion in the text. Important changes to TE errors are  
 436 marked with bold font in Table 1.

437 Various configurations are used and referred to in terms of the *COMPSET* (Com-  
 438 ponent Set) value used in CESM2.1. The *COMPSET F2000climo* configuration refers  
 439 to 'real-world' AMIP (Atmospheric Model Intercomparison Project) type simulations us-  
 440 ing perpetual year 2000 SST (Sea Surface Temperature) boundary conditions. The first 7  
 441 simulations in the table (those above the horizontal line) are such AMIP-type simulations  
 442 (F2000climo) with the first serving as a control for the 6 following variants. The remain-  
 443 ing 5 simulation descriptors (below the horizontal line in Table 1) list their *COMPSET* or  
 444 dynamical core settings.

445 The different configurations listed below (and discussed in separate sub-sections) are  
 446 chosen to assess TE errors associated with different aspects of the dynamical core numer-  
 447 ical algorithm, PDC method, surface conditions, etc. (as pointed out in parenthesis at the  
 448 end of each item listing):

- 449 • *TE consistent*: The TE consistent version uses *state update* physics-dynamics cou-  
 450 pling (*fctype* 1) described in section 3.1 (this configuration does not have PDC  
 451 errors and it has the same TE definition in physics and dynamics; and hence the  
 452 energetically most consistent setup in terms of least number of TE error terms),
- 453 • '*dribbling*' A: as *TE consistent* but with *dribbling* physics-dynamics coupling (*fctype*  
 454 0) (section 3.2; this setup is used to assess PDC errors),
- 455 • '*dribbling*' B: as *TE consistent* but with *dribbling* combination physics-dynamics  
 456 coupling (*fctype* 2) (section 3.2; this setup is used to assess PDC errors),
- 457 • *vert limiter*: as *TE consistent* but using limiters in the vertical remapping of mo-  
 458 mentum (section 3.3; experiment is used to assess TE errors associated with shape-  
 459 preserving limiters in vertical remapping),
- 460 • *smooth topo*: as *TE consistent* but using smoother topography (see section 3.4; ex-  
 461 periment is used to assess TE sensitivity to surface roughness),
- 462 • *energy discr*: The version with energy discrepancy (but no physics-dynamics cou-  
 463 pling errors) described in section 3.5 (experiment is used to estimate energy dis-  
 464 crepancy errors),

**Table 1.** TE tendencies in units of  $W/m^2$  associated with various aspects of CAM-SF run in AMIP-type setup (unless otherwise noted). Column 1 is the identifier for the model configuration. See the text for a brief summary of these descriptors. They are defined in more detail in the following sections where the section titles also include the ‘Descriptor’ from Table 1 to make it easier for the reader to match Table entries with discussion in the text. Column 2 is  $N = \text{qsize\_condensate\_loading}$  identifying how many water species are thermodynamically/inertially active in the dynamical core (see section 2.1 for details). Column 3, 1cp\_moist, indicates whether or not the heat capacity includes water variables or not and column 4 shows physics-dynamics coupling method ftype. The TE tendencies  $\partial \widehat{E}$  in columns 5-14 are defined in section 2.4. If  $\partial \widehat{E}$  is less than  $10^{-5} W/m^2$  it is set to zero in the Table. Significant changes compared to the baseline (*TE consistent* configuration) discussed in the main text are in bold font. Entries marked with ‘-’ refer to TE tendencies that can not be directly calculated with the current framework, ‘not impl’ refers to energy diagnostics not implemented in FV dynamical core, and blank in *FHS94* refers to the fact that this setup is run without energy fixer (parameterization not consistent with energy fixer) and hence there are no energy fixer numbers.

Descriptor	$N$	1cp_moist	ftype	$\partial \widehat{E}_{\text{phys}}^{(pwork)}$	$\partial \widehat{E}_{\text{phys}}^{(efix)}$	$\partial \widehat{E}_{\text{phys}}^{(discr)}$	$\partial \widehat{E}_{\text{dyn}}^{(2D)}$	$\partial \widehat{E}_{\text{dyn}}^{(hvis)}$	$\partial \widehat{E}_{\text{dyn}}^{(heat)}$	$\partial \widehat{E}_{\text{dyn}}^{(res)}$	$\partial \widehat{E}_{\text{dyn}}^{(remap)}$	$\partial \widehat{E}_{\text{dyn}}^{(adiab)}$	$\partial \widehat{E}_{\text{dyn}}^{(pd)}$
<i>TE consistent</i>	1	false	1	0.312	0.300	0	-0.601	-0.608	0.565	0.007	-0.011	-0.613	0
‘dribbling’ A	1	false	0	0.315	0.313	0	-0.577	-0.584	0.568	0.007	-0.011	-0.588	<b>0.469</b>
‘dribbling’ B	1	false	2	0.316	0.341	0	-0.598	-0.606	0.563	0.008	-0.011	-0.609	<b>0.484</b>
<i>vert limiter</i>	1	false	1	0.317	0.472	0	-0.590	-0.597	0.509	0.006	<b>-0.199</b>	-0.789	0
<i>smooth topo</i>	1	false	1	0.315	<b>-0.008</b>	0	<b>-0.295</b>	<b>-0.300</b>	0.493	0.005	-0.012	<b>-0.307</b>	0
<i>energy discr</i>	5	true	1	0.332	-0.313	<b>0.594</b>	-0.603	-0.612	0.575	0.009	-0.011	-0.614	-
<i>default</i>	5	true	2	0.316	-0.272	-	-0.578	-0.587	0.579	0.010	-0.012	-0.589	-
<i>QPC6</i>	1	false	1	0.305	-0.169	0	<b>-0.129</b>	<b>-0.131</b>	0.477	0.001	-0.007	<b>-0.136</b>	0
<i>FHS94</i>	1	false	2	0	0	0	<b>-0.025</b>	<b>-0.025</b>	0.122	0	0.005	<b>-0.020</b>	-
<i>FV</i>	1	false	1	0.304	0.670	0	not impl.	not impl.	not impl.	not impl.	not impl.	<b>-0.974</b>	0
<i>CSLAM</i>	1	false	1	0.312	0.239	0	-0.547	-0.557	0.620	0.010	-0.011	-0.558	<b>-0.070</b>
<i>CSLAM default</i>	5	true	2	0.320	-0.342	-	-0.524	-0.537	0.641	0.013	-0.011	-0.535	-

- 465 • *default*: as *energy\_discr* version but with `ftype=2` which is the current default  
466 CAM-SE (section 3.5; we assess this configuration since it is the default CAM-SE  
467 configuration),
- 468 • *QPC6*: A simplified aqua-planet setup based on the *TE consistent*, i.e an aqua-  
469 planet setup using CAM6 physics; an ocean covered planet in perpetual equinox,  
470 with fixed, zonally symmetric sea surface temperatures [Neale and Hoskins, 2000;  
471 Medeiros et al., 2016] (section 3.6; experiment is used to assess TE errors in a sim-  
472 plified moist environment),
- 473 • *FSH94*: Dry dynamical core configuration based on Held-Suarez forcing which  
474 relaxes temperature to a zonally symmetric equilibrium temperature profile and  
475 simple linear drag at the lower boundary [Held and Suarez, 1994] (section 3.7; ex-  
476 periment is used to assess if TE errors in one of the simplest climate test cases is  
477 representative of full model TE errors),
- 478 • *FV*: A configuration with the SE dynamical core replaced with the finite-volume  
479 core (section 3.8; experiment is used to assess TE errors of a different dynamical  
480 core), and
- 481 • *CSLAM*: The quasi equal-area physics grid configuration of CAM-SE based on the  
482 TE consistent setup (section 3.9; used to assess TE errors associated with separat-  
483 ing the dynamics grid from the physics grid)
- 484 • *CSLAM default*: Same as *CSLAM* configuration but with `ftype=2` and all forms of  
485 water thermodynamically/inertially active in the dynamical core (setup is evaluated  
486 since it is the default CAM-SE-CSLAM setup).

### 493 3.1 *TE consistent: state-update physics-dynamics coupling (ftype=1) and no TE* 494 *formula discrepancy*

495 This configuration is the most energetically consistent in that the physical parame-  
496 terizations and the continuous equations of motion on which the dynamical core is based,  
497 conserve the same TE (defined in equation (8)); and there are no spurious sources/sinks  
498 in physics-dynamics coupling. Energetic consistency in dynamics and physics is obtained  
499 by setting  $c_p^{(\ell)} \equiv c_p^d$  and  $\mathcal{L}_{all} = \{\text{'d', 'wv'}\}$  in the dynamical core equations of motion  
500 and TE computations. Associated namelist changes resulting in this configuration are  
501 `lcp_moist = .false.`, `se_qsize_condensate_loading = 1`, and `ftype = 1`. We use  
502 this configuration as a baseline since it has the least number of TE error terms ( $\partial \widehat{E}^{(pdc)} =$   
503  $\partial \widehat{E}^{(discr)} = 0$ ).

504 The TE consistent configuration in AMIP-type simulation (*F2000climo*) is used to  
505 compute baseline TE tendencies which will be used to compare with other model con-  
506 figurations. First we establish how long an average is needed to get robust TE tendency  
507 estimates. Figure 2 shows  $\partial \widehat{E}$  for various aspects of CAM-SE as a function of time. The  
508 simulation length is 5 years and monthly average values are used for the analysis. First  
509 consider the left plot. The TE tendency from parameterizations ( $\partial \widehat{E}_{phys}^{(param)}$ ) show signif-  
510 icant variability with an amplitude of approximately  $2.5W/m^2$ . As noted above this term  
511 does not figure in the spurious TE budget. The net source/sink provides an equal and op-  
512 posite term to balance it. That said, the variability is reflected onto the TE tendency due  
513 to pressure work error  $\partial \widehat{E}_{phys}^{(pwork)} \approx 0.32 \pm 0.08W/m^2$ . On the scale used in the left-  
514 hand plot the TE tendency of the adiabatic dynamical core  $\partial \widehat{E}_{dyn}^{(adiab)}$  does not seem to be  
515 affected by  $\partial \widehat{E}_{phys}^{(param)}$  or  $\partial \widehat{E}_{phys}^{(pwork)}$  in terms of variability, and remains stable at approxi-  
516 mately  $-0.6W/m^2 \pm 0.02W/m^2$ . The TE fixer, in this model configuration, fixes  $\partial \widehat{E}_{dyn}^{(adiab)}$   
517 and  $\partial \widehat{E}_{phys}^{(pwork)}$ . Since the TE imbalance in the adiabatic dynamics remains approximately  
518 constant and the TE tendency associated with pressure work error has variability, the TE  
519 tendency from the  $\partial \widehat{E}_{phys}^{(efix)}$  has variability;  $\partial \widehat{E}_{phys}^{(efix)} \approx 0.30 \pm 0.08W/m^2$ . As a consistency

520 check  $-\partial\hat{E}_{dyn}^{(adiab)} - \partial\hat{E}_{phys}^{(pwork)}$  is plotted with asterisk's and they coincide (as expected)  
 521 with  $\partial\hat{E}_{phys}^{(efix)}$  fulfilling (23).

522 The right-hand plot in Figure 2 shows a breakdown of the dynamical core TE tendencies.  
 523 The majority of the TE errors are due to hyperviscosity on temperature and pressure,  
 $\partial\hat{E}_{dyn}^{(hvis)} \approx -0.61 \pm 0.01 W/m^2$ . The diffusion of momentum is added back as  
 524 frictional heating and is therefore not part of  $\partial\hat{E}_{dyn}^{(hvis)}$ . The frictional heating is a significant  
 525 term in the TE tendency budget  $\partial\hat{E}_{dyn}^{(fheat)} \approx 0.56 \pm 0.02 W/m^2$  and exhibits some variabil-  
 526 ity but with a rather small amplitude. The remaining TE error in the floating Lagrangian  
 527 dynamics is inviscid dissipation and time-truncation errors  $\partial\hat{E}_{dyn}^{(res)} = \partial\hat{E}_{dyn}^{(2D)} - \partial\hat{E}_{dyn}^{(hvis)} \approx$   
 528  $0.007 W/m^2$ . The TE tendency from vertical remapping is approximately  $\partial\hat{E}_{dyn}^{(remap)} \approx$   
 529  $-0.01 W/m^2$ . To within  $\sim 0.02 W/m^2$  the dynamical core TE tendency terms can be com-  
 530 puted from just one month average TE integrals. The TE tendencies computed in physics,  
 531 excluding  $\partial\hat{E}_{phys}^{(param)}$ , exhibit more variability and are only accurate to  $\sim 0.1 W/m^2$  after a  
 532 one month average.

533 While it is advantageous to use *state-update* physics-dynamics coupling algorithm  
 534 (`ftype=1`) in terms of having no spurious TE tendency from coupling,  $\partial\hat{E}^{(pdc)} = 0$ ,  
 535 it does result in spurious gravity waves in the simulations [see, e.g., Figure 5 in *Gross*  
 536 *et al.*, 2018]. Figure 3a shows a 1 year average of  $|\frac{dp_s}{dt}|$ , a measure of high frequency  
 537 gravity wave noise. It clearly exhibits unphysical oscillations coinciding with element  
 538 boundaries. Details of the spectral-element method, its coupling to physics and associ-  
 539 ated noise issues are discussed in detail in *Herrington et al.* [2018]. The noise in the sol-  
 540 utions is even visible in the 500hPa pressure velocity annual average (Figure 4a). This  
 541 issue can be alleviated by using a shorter physics time-step so that the physics increments  
 542 are smaller (not shown). Climate modelers have historically not pursued a shorter physics  
 543 time-step in production configurations as climate parameterizations are computationally  
 544 expensive and there is a large sensitivity to physics time-steps in the simulated climate  
 545 [e.g. *Williamson and Olson*, 2003; *Wan et al.*, 2015].

### 546 3.2 ‘dribbling’ A/B: Non-TE conservative physics-dynamics coupling (`ftype=0, 2`)

547 Before discussing the impact of different PDC methods on the TE budget, we dis-  
 548 cuss element boundary noise issues in CAM-SE which are related to PDC method. This  
 549 motivates the different PDC methods implemented in CAM-SE.

#### 553 3.2.1 Spurious element boundary noise from physics-dynamics coupling

554 When switching to *dribbling* physics-dynamics coupling algorithm (`ftype=0`) in  
 555 which the tendencies from physics are added throughout the dynamics (in this case twice  
 556 per physics time-step) then the noise issues described in previous section disappear (Figure  
 557 3b and 4b). That said, there is a significant issue with this approach; the tracer mass bud-  
 558 get may not be closed. How this comes about is illustrated in Figure 5 and explained in  
 559 the next paragraph.

560 The orange curve on Figure 5a, b, d, and e is the initial state of, e.g., cloud liq-  
 561 uid mixing ratio as a function of location, e.g., longitude. Cloud liquid is zero outside  
 562 of clouds and hence provides a good example for the purpose of this illustration. The  
 563 light blue arrows show the increments (in terms of length of arrow) computed by the  
 564 parameterizations based on the initial state and scaled for the partial update with *dribbling*  
 565 (`ftype=0`). With *state-update* (`ftype=1`) the increments from physics are added to the  
 566 dynamical core state (dotted line on 5b) before the dynamical core advances the solution  
 567 in time. The parameterizations are designed to not drive the mixing ratios negative so the  
 568 state-update in dynamics will not generate negatives (or overshoots). Then the dynami-  
 569 cal core advects the distribution (solid curve on Figure 5c). With *dribbling* (`ftype=0`) the

physics increments are split into equal chunks (in this illustration two; blue errors on Figure 5d). Half of the physics increments are added to the initial state (dotted line on Figure 5e) and then dynamics advects the distribution half of the total dynamical core steps (dashed line on Figure 5e). Then the other half of the physics increments are applied (in the same location as they were computed by physics). Now after the previous/first advection step the cloud liquid distribution has moved and the mixing ratio may be zero (or less than the increment prescribed by physics) where the physics forcing is applied (e.g., left side of dashed curve). Hence the physics increment is driving the mixing ratios negative in those locations. Thereafter the distribution is advected (solid curve on Figure 5f). In CAM the increments added in the dynamical core are limited so that they drive the mixing to zero (but not negative) if this problem occurs. This leads to a net source of mass compared to the mass change that the parameterizations prescribe (see Figure 6). Although the average source of mass is small each time-step it always has the same sign (i.e. it is a bias) and therefore accumulates. *Zhang et al.* [2018] estimated that this spurious source of mass is equivalent to  $\sim 10\text{cm}$  sea-level rise per decade in coupled climate simulation experiments.

The majority of the noise with *state-update* (`ftype=1`) physics-dynamics coupling method comes from momentum sources/sinks and heating/cooling. A way to alleviate noise problems and, at the same time, close the tracer mass budgets (in physics-dynamics coupling) is to use *state-update* (`ftype=1`) coupling for tracers and *dribbling* (`ftype=0`) coupling for momentum and temperature (referred to as *combination*, `ftype=2`). Figure 3c shows the noise diagnostic  $|\frac{dp_s}{dt}|$  for *combination* (`ftype=2`) coupling. Figure 3c looks very similar to Figure 3b but there is some noise near element boundaries. That said, in terms of vertical pressure velocities *combination* (`ftype=2`) and *dribbling* (`ftype=0`) climates are similar in terms of the level of noise (Figure 4b and 4c). The element noise in CAM-SE with *combination* (`ftype=2`) seen in both  $|\frac{dp_s}{dt}|$  and 500hPa pressure velocity can be ‘removed’ by using CAM-SE-CSLAM (Figure 3d) which uses a quasi equal-area physics grid and CSLAM [Conservative Semi-Lagrangian Multi-tracer; *Lauritzen et al.*, 2010] consistently coupled to the SE method [*Lauritzen et al.*, 2017]. The noise patterns in vertical velocity off the western coast of South America are present in all CAM-SE simulations (and hence not related to physics-dynamics coupling algorithm) are also ‘removed’ by using CAM-SE-CSLAM [*Herrington et al.*, 2018].

### 3.2.2 Spurious TE tendencies from physics-dynamics coupling

When using the same TE formula in the dynamical core and physics the spurious TE tendency from physics-dynamics coupling can be assessed. As described in item 5 (Section 2.3), PDC errors can be attributed to underlying pressure changes during the ‘dribbling’ of temperature and velocity component increments as well as PDC ‘clipping’ errors in the water variables (the process in which ‘clipping’ occurs is described in detail in the previous subsection). The TE error associated with ‘clipping’ PDC error occurs when the mass-change prescribed by physics that is consistent with the fluxes in/out of the physics column does not equal the actual mass change applied to the dynamical core state due to ‘clipping’

For `ftype=2` PDC only the increment for temperature and momentum are *dribbled* whereas tracer mass is state-updated (no ‘clipping’ errors). This results in a spurious PDC TE tendency of  $\partial \widehat{E}^{(pdc)} = -0.484\text{W/m}^2$ . When using `ftype=0` PDC also tracer increments are *dribbled* (hence there are ‘clipping’ PDC errors) a similar TE tendency results  $\partial \widehat{E}^{(pdc)} = -0.469\text{W/m}^2$ . The difference between the TE PDC tenendency for `ftype=2` and `ftype=0` provides an estimate of the TE PDC ‘clipping’ error. The ‘clipping’ PDC TE tenendency is very small  $0.015\text{W/m}^2$ .

### 619      3.3 *vert limiter*: Limiters on vertical remapping of momentum

620      CAM-SE uses a floating Lagrangian vertical coordinate [Starr, 1945; Lin, 2004]  
 621 which requires the remapping of the atmospheric state from floating levels back to refer-  
 622 ence levels to maintain computational stability and to provide state data consistent with  
 623 the physics formulation. The mapping algorithm is based on the mass conservative PPM  
 624 (Piecewise Parabolic Method) with options for shape-preserving limiters. In CAM-SE mo-  
 625 mentum components and internal energy are used as the variables mapped in the vertical  
 626 [Lauritzen *et al.*, 2018] and, contrary to earlier versions of CAM-SE, there is no limiter  
 627 on the remapping of wind components. If the shape-preserving limiter is used for mo-  
 628 mentum mapping then the TE dissipation increases by over an order of magnitude from  
 629  $\sim 0.01W/m^2$  to  $\sim 0.2W/m^2$  (Table 1).

### 630      3.4 *smooth topo*: Smoother topography

631      Topography for CAM is generated using a new version of the software/algorith described in Lauritzen *et al.* [2015] that is available at <https://github.com/NCAR/Topo>.  
 632 The updates to the software includes smoothing algorithms and the computation of sub-  
 633 grid-scale orientation of topography.

635      The default topography in CAM-SE uses the same amount of topography smoothing as CAM-FV (distance weighted smoother applied to the raw topography on  $\sim 3\text{km}$   
 636 cubed-sphere grid with a smoothing radius of 180km referred to as C60). When the to-  
 637 topography is smoother (in this case using C92 smoothing, i.e. smoothing radius of approx-  
 638 imately 276km) the hyperviscosity operators are less active leading to reduced TE errors,  
 639 i.e.  $\partial\widehat{E}_{dyn}^{(hvis)}$  is reduced in half from approximately  $-0.6W/m^2$  to  $-0.3W/m^2$ . The vertical  
 640 remapping TE error, however, remains approximately the same. Since the pressure work  
 641 error is approximately  $0.3W/m^2$  it almost exactly compensates for the TE tendency from  
 642 the dynamical core  $\partial\widehat{E}_{dyn}^{(adiab)}$ . Hence if one would only diagnose the TE tendency from  
 643 the energy fixer one could mistakenly conclude that the model universally conserves TE  
 644 when, in fact, there are compensating TE errors in the system. These compensating errors  
 645 can only be diagnosed through a careful breakdown of the total TE tendencies.  
 646

### 647      3.5 *default*: TE formula discrepancy errors

648      To assess the TE errors due to the discrepancy in the energy formula used by dy-  
 649 namics and physics, a simulation using *state-updating* (*ftype*=1, no ‘dribbling’ errors) and  
 650 thermodynamically/inertially active condensates in the dynamical core (*qsize\_condensate\_loading* =  
 651 5) and consistent/accurate associated heat capacities  $c_p^{(\ell)}$  (namelist *1cp\_moist=.true.*)  
 652 has been performed. In this setup the continuous equations of motion in the dynami-  
 653 cal core conserve an energy different from physics, and the energy fixer will restore the  
 654 ‘physics’ version of energy. Despite the dynamical core now using a more comprehensive  
 655 formula for energy, the TE dissipation terms in the dynamical core are roughly the same  
 656 as in the energy consistent versions of the model. Using (26) we can assess the TE energy  
 657 discrepancy errors which result in  $\sim 0.59W/m^2$ . Taylor [2011] found a similar result just  
 658 from using the more comprehensive formula for heat capacity (based on dry air and water  
 659 vapor) and not including thermodynamically/inertially active condensates. As noted before  
 660 this formulation inconsistency is due to the evolutionary nature of CAM development and  
 661 it is the intention to remove this inconsistency in future versions of the model.

662      The default version of CAM-SE uses this configuration but with *combination* (*ftype*=2)  
 663 which has similar TE characteristics (see Table 1). That said, the physics-dynamics cou-  
 664 pling error from *dribbling* momentum and temperature tendencies and the energy discrep-  
 665 ancy errors can not be separated in this configuration:

$$\partial\widehat{E}^{(pdc)} + \partial\widehat{E}^{(discr)} = 0.546W/m^2, \quad (27)$$

666 using (23). With *state-updating* (*ftype*=1) (i.e.  $\partial\widehat{E}^{(pdc)} = 0$ ) the energy discrepancy error  
 667 was  $0.594W/m^2$  and in the energy consistent setup (i.e.  $\partial\widehat{E}^{(discr)} = 0$ ) but using *dribbling*  
 668 (*ftype*=2) we got  $\partial\widehat{E}^{(pdc)} = 0.484W/m^2$ . So if the physics-dynamics coupling errors  
 669 and energy discrepancy errors in the different configurations would be additive, one would  
 670 have expected  $\partial\widehat{E}^{(pdc)} + \partial\widehat{E}^{(discr)}$  to be over  $1W/m^2$  which is clearly not the case (27).  
 671 Again, it must be concluded that there are canceling errors in the system.

### 672 **3.5.1 2D structure of TE errors**

673 Figure 7 shows the two-dimensional spatial structure of column-integrated TE ten-  
 674 dencies for the *default* configuration. The first plot (Figure 7a) shows column inte-  
 675 grated  $\partial E^{(param)}$ , i.e. the spatial structure of the ‘physical’ TE tendency. Only contours  
 676 from  $\pm 150W/m^2$  are shown although the actual range (noted above color bar) is  $-148.3W/m^2$   
 677 to  $1770W/m^2$ . The larger positive values occur only at a small number of grid points  
 678 (e.g., mountains of New Guinea). The column-integrated dynamical core TE tendency  
 679  $\partial\widehat{E}^{(adiab)}$  (Figure 7c) approximately balances  $\partial E^{(param)}$ ; this is expected in an AMIP  
 680 simulation that, if integrated long enough, should reach radiative equilibrium. The TE  
 681 pressure work error tendency  $\partial E^{(pwork)}$  (Figure 7b) is, as expected, largest where pre-  
 682 cipitation and evaporation is largest. The last 3 plots show terms in the dynamical core  
 683 budget: column-integrated TE tendency from the 2D adiabatic dynamical core,  $\partial\widehat{E}^{(2D)}$ ,  
 684 vertical remapping,  $\partial\widehat{E}^{(remap)}$ , and frictional heating,  $\partial\widehat{E}^{(fheat)}$ . The adiabatic dynamical  
 685 core TE tendency is dominated by the tendencies from the floating Lagrangian (quasi-  
 686 horizontal) dynamics. The frictional heating TE tendency is largest over/near topography.  
 687 Similarly for vertical remapping but, in addition, there are large TE tendencies in areas of  
 688 large updrafts/downdrafts over ocean.  
 689

### 694 **3.6 QPC6: Simplified surface**

695 By running the model in aqua-planet configuration one can assess the effect of sim-  
 696 plifying the surface boundary condition. In particular, without topography forcing the dy-  
 697 namical core is not challenged with respect to stationary near-grid-scale forcing. The TE  
 698 tendency with respect to pressure work error remains the same  $\partial\widehat{E}_{phys}^{(pwork)}$  as the AMIP-  
 699 type simulations, however, the adiabatic dynamical core TE tendency reduces to  $\partial\widehat{E}_{dyn}^{(adiab)} =$   
 700  $-0.14W/m^2$  (approximately a factor 4 reduction). Most of that reduction is due to viscos-  
 701 ity  $\partial\widehat{E}_{dyn}^{(hvis)} = -0.13W/m^2$ . The frictional heating is roughly the same as AMIP  $\partial\widehat{E}_{dyn}^{(fheat)} =$   
 702  $0.48W/m^2$  as is the vertical remapping  $\partial\widehat{E}_{dyn}^{(remap)} = -0.01W/m^2$ . To evaluate the dynam-  
 703 ical cores diffusion of TE it is therefore important to asses the model in a configuration  
 704 with topography as the wave dynamics generated by topography leads to more active dif-  
 705 fusion operators.

### 706 **3.7 FHS94: Simplified physics (no moisture)**

707 Simplifying the setup even further by replacing the parameterizations with relax-  
 708 ation towards a zonally symmetric temperature profile and simple boundary layer friction  
 709 (Held-Suarez forcing) as well as excluding moisture, the TE errors in the dynamical core  
 710 decreases even further to  $\sim 0.002W/m^2$  since there is no small scale forcing. Small scales  
 711 are only created by the nonlinear dynamics and the physics works to damp them. Hyper-  
 712 viscosity is less active leading to significant reductions compared to aqua-planet and ‘real-  
 713 world’ simulation results. The TE diffusion in vertical remapping reduces by an order of  
 714 magnitude compared to the aqua-planet simulations ( $\sim 0.0005W/m^2$ ). This further em-  
 715 phasizes that TE diffusion assessment in a simplified setup is not necessarily telling for  
 716 the dynamical cores performance with moist physics and topography that challenge the  
 717 dynamical core in terms of strong grid-scale forcing.

### 718 3.8 FV: Changing dynamical core to Finite-Volume (FV)

719 As a comparison the TE error characteristics of the CAM-FV dynamical core are  
 720 assessed. Although the TE diagnostics have not been implemented in the CAM-FV dy-  
 721 namical core, the TE diagnostics in CAM physics are independent of dynamical core  
 722 and can therefore be activated with CAM-FV. The CAM-FV dynamical core uses *state-*  
 723 *update* physics-dynamics coupling (`ftype=1`) ( $\partial\widehat{E}^{(pdc)} = 0$ ) and the same TE definition  
 724 as CAM physics ( $\partial\widehat{E}^{(discr)} = 0$ ). Hence (24) can be used to compute the TE errors of  
 725 the CAM-FV dynamical core,  $\partial\widehat{E}_{dyn}^{(adiab)} \approx -1W/m^2$ . As we do not have the breakdown  
 726 of  $\partial\widehat{E}_{dyn}^{(adiab)}$  it can not be determined how much of the TE errors are due to the vertical  
 727 remapping. Furthermore, CAM-FV contains intrinsic dissipation operators (limiters in the  
 728 flux operators) making it difficult to assess TE sources/sinks due to dissipation. Note that  
 729 the pressure work error even with a change of dynamical core remains approximately the  
 730 same as the CAM-SE configurations.

### 731 3.9 CSLAM: Quasi equal-area physics grid

732 This configuration was discussed in the context of element noise in section 3.2.1.  
 733 By averaging the dynamics state of an equal-partitioning (in central angle cubed-sphere  
 734 coordinates) of the elements, the element-boundary noise found in CAM-SE can be re-  
 735 moved. Lauritzen *et al.* [2018] argue that this way of computing the state for the physics  
 736 is more consistent with physics in terms of providing a cell-averaged state instead of ir-  
 737 regularly spaced point (quadrature) values. In order to achieve a closed mass-budget, this  
 738 configuration uses CSLAM for tracer transport rather than SE transport. That said, the  
 739 physics columns no longer coincide with the quadrature grid and there are TE errors asso-  
 740 ciated with mapping state and tendencies between the two grids.

741 In this configuration the energy diagnostics computed in the dynamical core are  
 742 computed on the quadrature grid and the energy diagnostics computed in physics are on  
 743 the physics grid. If the TE consistent configuration is used (`ftype=1, qsize_condensate_loading=1,`  
 744 `lcp_moist=.false.`) then the physics-dynamical coupling errors,  $\widehat{E}^{(pdc)}$  computed with  
 745 (21), are entirely due to mapping state from quadrature grid to physics grid and map-  
 746 ping tendencies back the quadrature grid from the physics grid. The results is  $\widehat{E}^{(pdc)} =$   
 747  $-0.07W/m^2$  which is a rather small error compared to other terms in the TE budget.

748 Due to similar noise problems with CAM-SE-CSLAM when using `ftype=1` that  
 749 were observed in CAM-SE (Figure 3 and 4), the default version of CAM-SE-CSLAM uses  
 750 `ftype=2`. Again physics-dynamics coupling errors and TE discrepancy errors can not be  
 751 separated;  $\partial\widehat{E}^{(pdc)} + \partial\widehat{E}^{(discr)} = 0.557W/m^2$ .

## 752 4 Conclusions

753 A detailed total energy (TE) error analysis of the Community Atmosphere Model  
 754 (CAM) using version 6 physics (included in the CESM2.1 release) running at approxi-  
 755 mately 1° horizontal resolution has been presented. In the global climate model there can  
 756 be many spurious contributions to the TE budget. These errors can be divided into four  
 757 categories: physical parameterizations, adiabatic dynamical core, the coupling between  
 758 physics and dynamics, and TE definition discrepancies between dynamics and physics.  
 759 The latter is not by design but through the evolutionary nature of model development. By  
 760 capturing the atmospheric state at various locations in the model algorithm, a detailed  
 761 budget of TE errors can be constructed. The net spurious TE energy errors are com-  
 762 pensated with a global energy fixer (providing a global uniform temperature increment) every  
 763 physics time-step.

764 In CAM physics the parameterizations have, by design, a closed energy budget (change  
 765 in TE is balanced by fluxes in/out the top and bottom of physics columns) if it is assumed

that pressure is not modified. However, the pressure changes due to fluxes of mass (e.g., water vapor) in/out of the column which changes energy (referred to as pressure work error). The pressure work error with the full moist physics configuration is very stable across different configurations at  $\sim 0.3W/m^2$ . The TE errors in the spectral element (SE) dynamical core varies across configurations. Aspects that influence TE is the presence of topography, the amount of topography smoothing and moist physics. By smoothing topography more the TE error is cut in half from  $\sim -0.6W/m^2$  to  $\sim -0.3W/m^2$ ; and reduces by a factor of six ( $\sim -0.1W/m^2$ ) if no topography is present at all (aqua-planet configuration). Moist physics forcing also contributes significantly to the TE budget. For example, in the dry Held-Suarez setup TE dissipation of the SE dynamical core reduces to  $-0.03W/m^2$ . Topography and moist physics force the dynamical core at the grid scale and hence the viscosity operators are more active. Consistent with this statement is that the changes in TE discussed so far are almost entirely due to the viscosity operator TE dissipation. For CAM-SE the spurious TE dissipation in the adiabatic dynamical core is  $\sim -0.6W/m^2$  in ‘real-world’ configurations. For comparison, CAM-FV’s spurious TE change due to the adiabatic dynamical core is  $\sim -1W/m^2$ .

By further breaking down the TE dissipation in the SE dynamical core it is observed the vertical remapping accounts for only  $\sim -0.01W/m^2$ . That said, if the shape-preserving limiters in the vertical remapping are invoked the TE dissipation increases 20-fold to  $\sim -0.2W/m^2$ . In CAM-SE the kinetic energy dissipation is added as heating in the thermodynamic equation (also referred to as frictional heating). The frictional heating remains very stable across configurations that include moisture ( $\sim 0.5W/m^2$ ) and reduces drastically for dry atmosphere setups (factor 4 reduction to  $(\sim 0.12W/m^2)$ ). Hence this term is an important term in the TE budget. The TE budget for the dynamical core is dominated by TE change due to hyperviscosity; TE errors due to time-truncation and frictionless equations of motion are negligible. Errors associated with physics-dynamics coupling (if applicable) are approximately  $0.5W/m^2$ . Due to the evolutionary nature of model development the SE dynamical core’s continuous equation of motion conserve a more comprehensive TE compared to the physical parameterizations. This TE discrepancy leads to an approximately  $0.5W/m^2$  total energy source. Running physics on a different grid than the dynamical introduces TE mapping errors such as in CAM-SE-CSLAM (Conservative Semi-Lagrangian Multi-tracer transport scheme). These errors are, however, rather small  $-0.07W/m^2$ .

A purpose of this paper is to better understand the energy characteristics of CAM and to encourage modeling groups to perform similar analysis to better understand the total energy flow in the atmospheric component of Earth system models. As has been demonstrated in this paper there can easily be compensating errors in the system which can not be identified without a detailed TE analysis. The analysis in this paper only considers  $1^\circ$  horizontal resolution and 32 levels in the vertical. The TE numbers and clipping results may not be accurate for other choices of horizontal and vertical resolutions.

## 806 Acknowledgments

We thank one anonymous reviewer, Hui Wan and Phil Rasch for their helpful comments that significantly improved the clarity of the manuscript. The National Center for Atmospheric Research is sponsored by the National Science Foundation. Computing resources (doi:10.5065/D6RX99HX) were provided by the Climate Simulation Laboratory at NCAR’s Computational and Information Systems Laboratory, sponsored by the National Science Foundation and other agencies. The data used to perform the energy analysis can be found at <https://github.com/PeterHjortLauritzen/2018-JAMES-energy>.

814 **References**

- 815 Boville, B. (2000), Toward a complete model of the climate system in Numerical Mod-  
 816 eling of the Global Atmosphere in the Climate System, in: P. Mote and A. O'Neill  
 817 (Eds.), *Numerical Modeling of the Global Atmosphere in the Climate system, Nu-*  
 818 *merical Modeling of the Global Atmosphere in the Climate System*, pp. 419–442, doi:  
 819 10.1007/978-3-642-11640-7\_12.
- 820 Computational and Information Systems Laboratory (2017), Cheyenne: HPE/SGI ICE XA  
 821 System (Climate Simulation Laboratory), Boulder, CO: National Center for Atmospheric  
 822 Research, doi:10.5065/D6RX99HX.
- 823 Eldred, C., and D. Randall (2017), Total energy and potential enstrophy conserv-  
 824 ing schemes for the shallow water equations using hamiltonian methods – part  
 825 1: Derivation and properties, *Geosci. Model Dev.*, 10(2), 791–810, doi:10.5194/  
 826 gmd-10-791-2017.
- 827 Gross, M., H. Wan, P. J. Rasch, P. M. Caldwell, D. L. Williamson, D. Klocke,  
 828 C. Jablonowski, D. R. Thatcher, N. Wood, M. Cullen, B. Beare, M. Willett, F. Lemarié,  
 829 E. Blayo, S. Malardel, P. Termonia, A. Gassmann, P. H. Lauritzen, H. Johansen, C. M.  
 830 Zarzycki, K. Sakaguchi, and R. Leung (2018), Physics-dynamics coupling in weather,  
 831 climate and earth system models: Challenges and recent progress, *Mon. Wea. Rev.*, 146,  
 832 3505–3544, doi:10.1175/MWR-D-17-0345.1.
- 833 Held, I. M., and M. J. Suarez (1994), A proposal for the intercomparison of the dynamical  
 834 cores of atmospheric general circulation models, *Bull. Amer. Meteor. Soc.*, 75, 1825–  
 835 1830.
- 836 Herrington, A. R., P. H. Lauritzen, M. A. Taylor, S. Goldhaber, B. E. Eaton, K. A. Reed,  
 837 and P. A. Ullrich (2018), Physics-dynamics coupling with element-based high-order  
 838 Galerkin methods: quasi equal-area physics grid, *Mon. Wea. Rev.*
- 839 Jablonowski, C., and D. L. Williamson (2011), The pros and cons of diffusion, filters  
 840 and fixers in atmospheric general circulation models, in: P.H. Lauritzen, R.D. Nair, C.  
 841 Jablonowski, M. Taylor (Eds.), *Numerical techniques for global atmospheric models,*  
 842 *Lecture Notes in Computational Science and Engineering*, Springer, 80, 381–493, doi:  
 843 10.1007/978-3-642-11640-7\_13.
- 844 Kasahara, A. (1974), Various vertical coordinate systems used for numerical weather pre-  
 845 diction, *Mon. Wea. Rev.*, 102(7), 509–522.
- 846 Lauritzen, P. H., R. D. Nair, and P. A. Ullrich (2010), A conservative semi-Lagrangian  
 847 multi-tracer transport scheme (CSLAM) on the cubed-sphere grid, *J. Comput. Phys.*,  
 848 229, 1401–1424, doi:10.1016/j.jcp.2009.10.036.
- 849 Lauritzen, P. H., J. T. Bacmeister, T. Dubos, S. Lebonnois, and M. A. Taylor (2014),  
 850 Held-Suarez simulations with the Community Atmosphere Model Spectral Element  
 851 (CAM-SE) dynamical core: A global axial angular momentum analysis using Eule-  
 852 rian and floating Lagrangian vertical coordinates, *J. Adv. Model. Earth Syst.*, 6, doi:  
 853 10.1002/2013MS000268.
- 854 Lauritzen, P. H., J. T. Bacmeister, P. F. Callaghan, and M. A. Taylor (2015), NCAR\_Topo  
 855 (v1.0): NCAR global model topography generation software for unstructured grids,  
 856 *Geosci. Model Dev.*, 8(12), 3975–3986, doi:10.5194/gmd-8-3975-2015.
- 857 Lauritzen, P. H., M. A. Taylor, J. Overfelt, P. A. Ullrich, R. D. Nair, S. Goldhaber, and  
 858 R. Kelly (2017), CAM-SE-CSLAM: Consistent coupling of a conservative semi-  
 859 lagrangian finite-volume method with spectral element dynamics, *Mon. Wea. Rev.*,  
 860 145(3), 833–855, doi:10.1175/MWR-D-16-0258.1.
- 861 Lauritzen, P. H., R. Nair, A. Herrington, P. Callaghan, S. Goldhaber, J. Dennis, J. T.  
 862 Bacmeister, B. Eaton, C. Zarzycki, M. A. Taylor, A. Gettelman, R. Neale, B. Dobbins,  
 863 K. Reed, and T. Dubos (2018), NCAR release of CAM-SE in CESM2.0: A reformula-  
 864 tion of the spectral-element dynamical core in dry-mass vertical coordinates with com-  
 865 prehensive treatment of condensates and energy, *J. Adv. Model. Earth Syst.*, 10(7), 1537–  
 866 1570, doi:10.1029/2017MS001257.

- 867 Lin, S.-J. (2004), A 'vertically Lagrangian' finite-volume dynamical core for global mod-  
868 els, *Mon. Wea. Rev.*, *132*, 2293–2307.
- 869 McRae, A. T. T., and C. J. Cotter (2013), Energy- and enstrophy-conserving schemes for  
870 the shallow-water equations, based on mimetic finite elements, *Quart. J. Roy. Meteor.  
Soc.*, *140*(684), 2223–2234, doi:10.1002/qj.2291.
- 872 Medeiros, B., D. L. Williamson, and J. G. Olson (2016), Reference aquaplanet climate in  
873 the community atmosphere model, version 5, *J. Adv. Model. Earth Syst.*, *8*(1), 406–424,  
874 doi:10.1002/2015MS000593.
- 875 Neale, R. B., and B. J. Hoskins (2000), A standard test for AGCMs including their phys-  
876 ical parametrizations: I: the proposal, *Atmos. Sci. Lett.*, *1*(2), 101–107, doi:10.1006/asle.  
877 2000.0022.
- 878 Neale, R. B., C.-C. Chen, A. Gettelman, P. H. Lauritzen, S. Park, D. L. Williamson, A. J.  
879 Conley, R. Garcia, D. Kinnison, J.-F. Lamarque, D. Marsh, M. Mills, A. K. Smith,  
880 S. Tilmes, F. Vitt, P. Cameron-Smith, W. D. Collins, M. J. Iacono, R. C. Easter, S. J.  
881 Ghan, X. Liu, P. J. Rasch, and M. A. Taylor (2012), Description of the NCAR Commu-  
882 nity Atmosphere Model (CAM 5.0), *NCAR Technical Note NCAR/TN-486+STR*, National  
883 Center of Atmospheric Research.
- 884 Skamarock, W. C., J. B. Klemp, M. G. Duda, L. Fowler, S.-H. Park, and T. D. Ringler  
885 (2012), A multi-scale nonhydrostatic atmospheric model using centroidal Voronoi tes-  
886 selations and C-grid staggering, *Mon. Wea. Rev.*, *240*, 3090–3105, doi:doi:10.1175/  
887 MWR-D-11-00215.1.
- 888 Starr, V. P. (1945), A quasi-Lagrangian system of hydrodynamical equations., *J. Atmos.  
Sci.*, *2*, 227–237.
- 889 Taylor, M. A. (2011), Conservation of mass and energy for the moist atmospheric prim-  
890 itive equations on unstructured grids, in: P.H. Lauritzen, R.D. Nair, C. Jablonowski,  
891 M. Taylor (Eds.), Numerical techniques for global atmospheric models, *Lecture Notes  
in Computational Science and Engineering*, Springer, *80*, 357–380, doi:10.1007/  
892 978-3-642-11640-7\_12.
- 893 Thuburn, J. (2008), Some conservation issues for the dynamical cores of NWP and cli-  
894 mate models, *J. Comput. Phys.*, *227*, 3715–3730.
- 895 Trenberth, K. E., and J. T. Fasullo (2018), Applications of an updated atmospheric ener-  
896 getics formulation, *J. Climate*, *31*(16), 6263–6279, doi:10.1175/JCLI-D-17-0838.1.
- 897 Wan, H., P. J. Rasch, M. A. Taylor, and C. Jablonowski (2015), Short-term time step con-  
898 vergence in a climate model, *J. Adv. Model. Earth Syst.*, *7*(1), 215–225, doi:10.1002/  
899 2014MS000368.
- 900 Williamson, D. L. (2002), Time-split versus process-split coupling of parameterizations  
901 and dynamical core, *Mon. Wea. Rev.*, *130*, 2024–2041.
- 902 Williamson, D. L., and J. G. Olson (2003), Dependence of aqua-planet simulations on  
903 time step, *Q. J. R. Meteorol. Soc.*, *129*(591), 2049–2064.
- 904 Williamson, D. L., J. G. Olson, C. Hannay, T. Toniazzo, M. Taylor, and V. Yudin (2015),  
905 Energy considerations in the community atmosphere model (cam), *J. Adv. Model. Earth  
906 Syst.*, *7*(3), 1178–1188, doi:10.1002/2015MS000448.
- 907 Zhang, K., P. J. Rasch, M. A. Taylor, H. Wan, R. Leung, P.-L. Ma, J.-C. Golaz, J. Wolfe,  
908 W. Lin, B. Singh, S. Burrows, J.-H. Yoon, H. Wang, Y. Qian, Q. Tang, P. Caldwell,  
909 and S. Xie (2018), Impact of numerical choices on water conservation in the E3SM  
910 atmosphere model version 1 (EAMv1), *Geosci. Model Dev.*, *11*(5), 1971–1988, doi:10.  
911 5194/gmd-11-1971-2018.
- 912

```

do nt=1,ntotal

PARAMETERIZATIONS:
Last dynamics state received from dynamics
output 'pBF'
efix Energy fixer
output 'pBP'
phys param Physics updates the state and state saved for energy fixer
output 'pAP'
pwork Pressure work (dry mass correction)
output 'pAM'
Physics tendency (forcing) passed to dynamics

DYNAMICAL CORE
output 'dED'
do ns=1,nsplit
output 'dAF'

phys
START PHYSICS-DYNAMICS COUPLING
Update dynamics state with (1/nsplit) of physics tendency (ftype=2)
if (ns=1) Update dynamics state with entire physics tendency (ftype=1)
DONE PHYSICS-DYNAMICS COUPLING

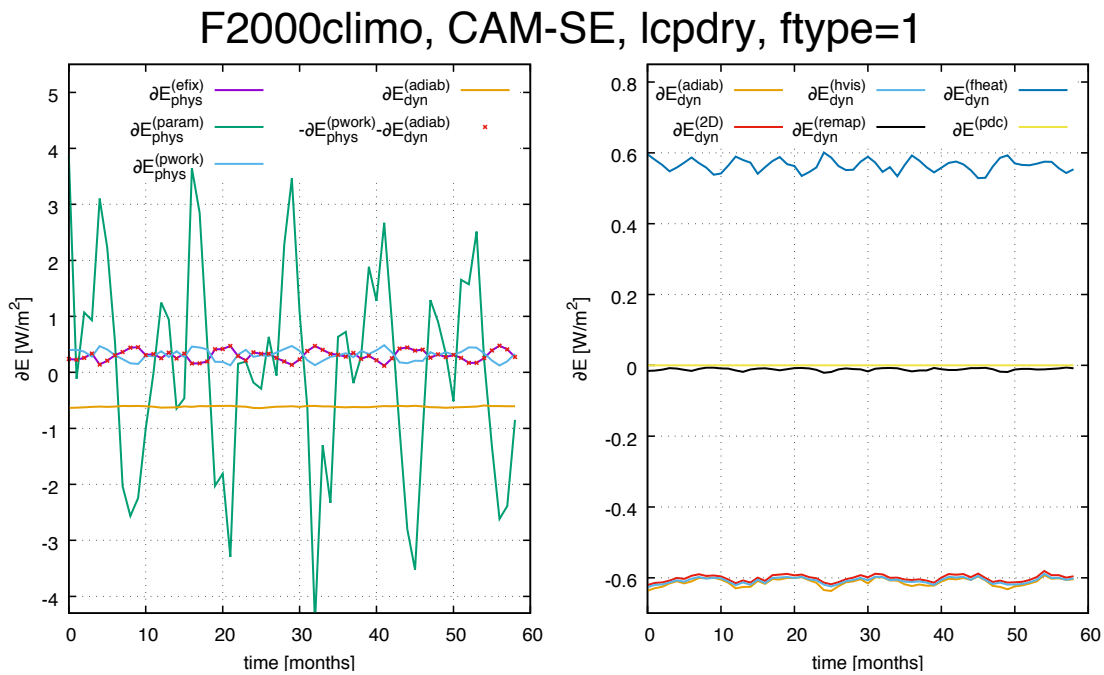
output 'dB'D'

adiab
2D
hvis
do nr=1,rsplit
Advance the adiabatic frictionless equations of motion
in floating Lagrangian layer
do ns=1,hypervis_subcycle
output 'dBH'
Apply hyperviscosity operators
output 'dCH'
fheat Add frictional heating to temperature
output 'dAH'
end do (ns=1,hypervis_subcycle)
end do (nr=1,rsplit)
output 'dAD'
remap
Vertical remapping from floating Lagrangian levels to Eulerian levels
output 'dAR'
end do (ns=1,nsplit)
Dynamics state saved for next model time step and passed to physics
output 'dB'F'

end do (nt=1,ntotal)

```

316 **Figure 1.** Pseudo-code for CAM-SE showing the order in which relevant physics updates are performed as  
 317 well as dynamical core steps and associated loops. In green font locations where the state is captured and out-  
 318 put is shown together with its 3 character identifier. The outer most loop (1, *ntotal*) advances the entire model  
 319  $\Delta t_{phys}$  seconds (in this case 1800s). The dynamical core loops are as follows: the outer loop is the vertical  
 320 remapping loop (1, *nsplit*) with associated time-step  $\Delta t_{phys}/nsplit$ . For stability the temporal advance-  
 321 ment of the equations of motion in the Lagrangian layer needs to be sub-cycled *rsplit* times. Within the  
 322 *rsplit*-loop the hyperviscosity time-stepping is sub-cycled *hypervis\_subcycle* times (again for stability).  
 323 For more details on the time-stepping in CAM-SE see Lauritzen *et al.* [2018].



487 **Figure 2.** Monthly averaged TE tendencies as a function of time for various aspects of the TE consistent  
 488 configuration of CAM-SE run in AMIP-type configuration with perpetual year 2000 SSTs. Left Figure shows  
 489  $\partial \hat{E}$  TE tendencies in physics and, for comparison, TE tendency for the adiabatic dynamical core. The right  
 490 plot shows the breakdown of  $\partial \hat{E}$  for the dynamical core. These plots show that the energy tendency from the  
 491 dynamical core is quite constant (to within  $\sim 0.02 W/m^2$  or less) so only one month simulations is adequate to  
 492 assess energy diagnostics for the dynamical core. For more details see Section 3.1.

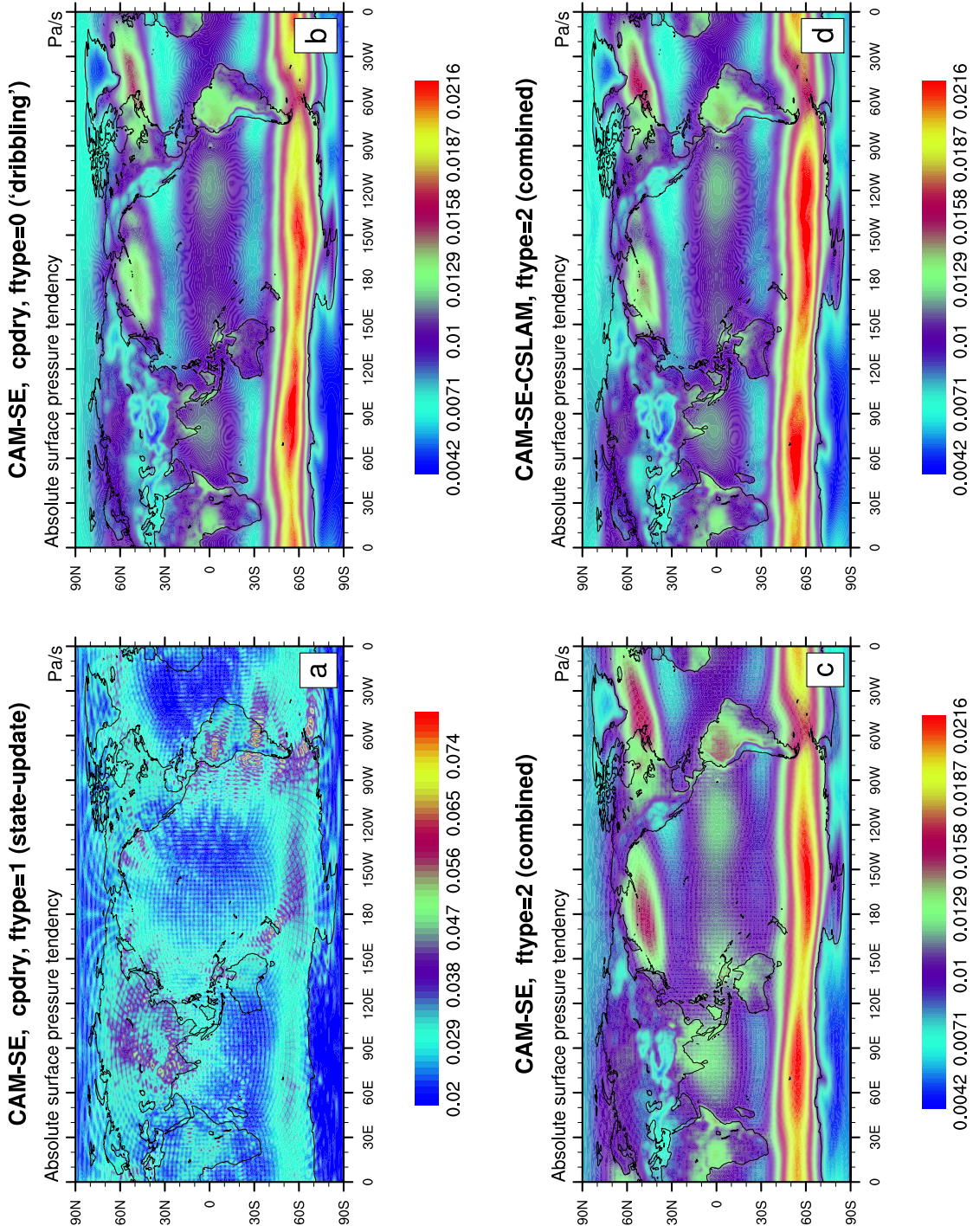


**Figure 3.** One year average of the absolute surface pressure tendency for (a) the TE consistent configuration, (b) ‘dribbling’ physics-dynamics coupling, (c) ftype=2 physics-dynamics coupling and (d) CSLAM version of CAM-SE, respectively. (a) has a closed physics-dynamics coupling budget but spurious noise, (b) has no spurious noise but the mass-budget in physics-dynamics coupling is not closed (see Figure 6), (c) has a closed mass budget in physics-dynamics coupling but some spurious noise at element boundaries which is eliminated when using CAM-SE-CSLAM (d). Note, the smallest value in panel (a) is the largest in panels (b), (c) and (d).

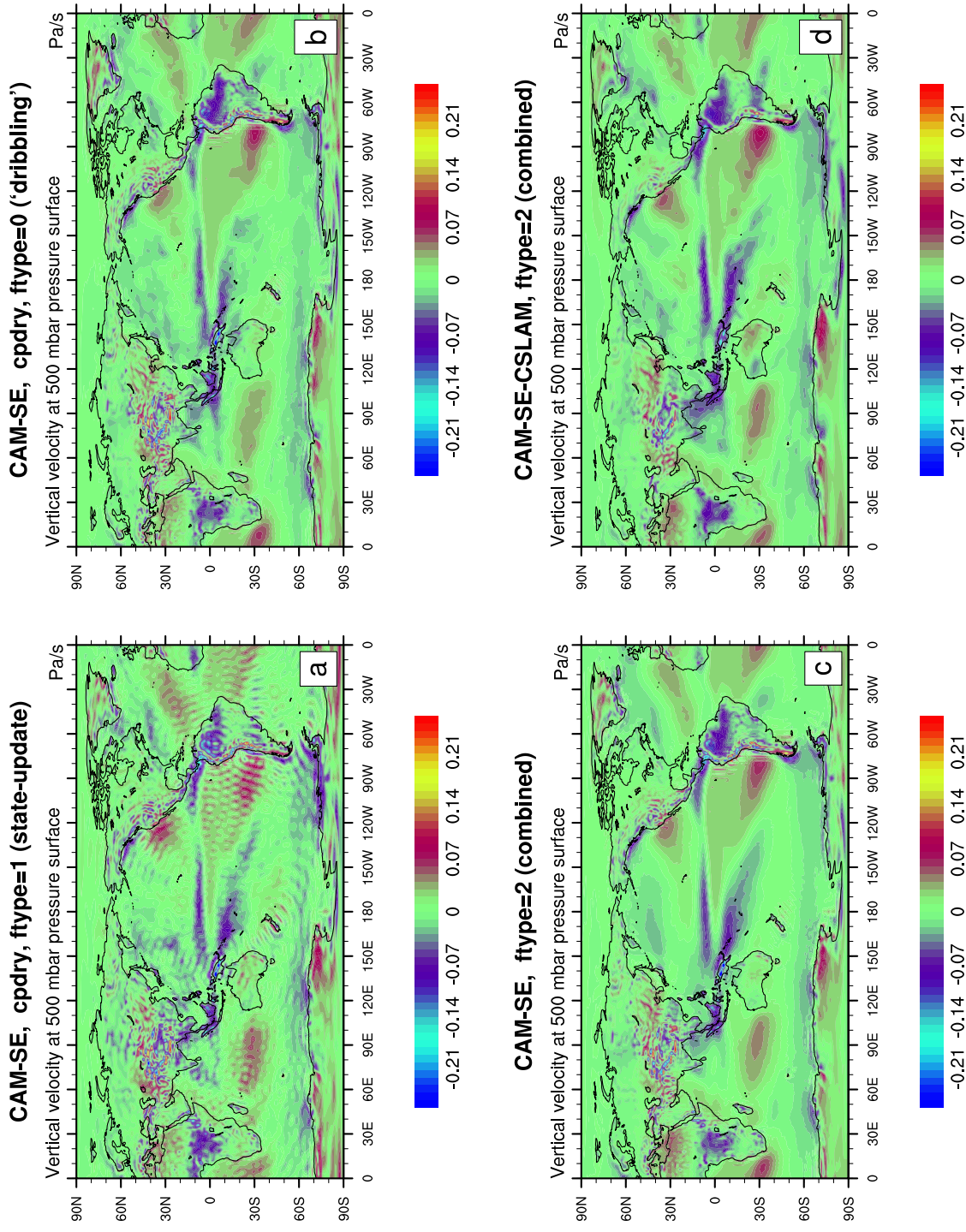


**Figure 4.** Same as Figure 3 but for 500hPa vertical pressure velocity. Note the ringing patterns off the West coast of South America and around the Himalayas in CAM-SE (a-c) that are eliminated with CAM-SE-CSLAM (d) that makes use of a quasi equal-area physics grid.

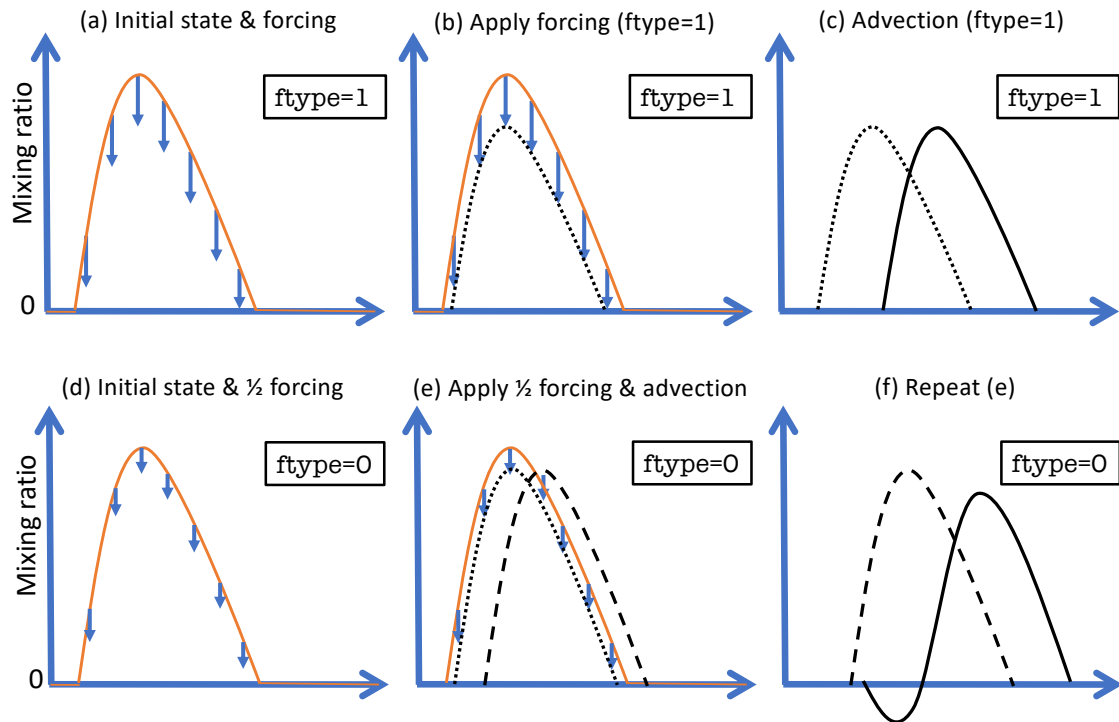


**Figure 5.** A schematic of state-update ( $\text{ftype}=1$ ; row 1) and ‘dribbling’ ( $\text{ftype}=0$ ; row 2) physics-dynamics coupling algorithms. See Section 3.2 for details.

## F2000climo, CAM-SE, cpdry, ftype=0 ('dribbling')

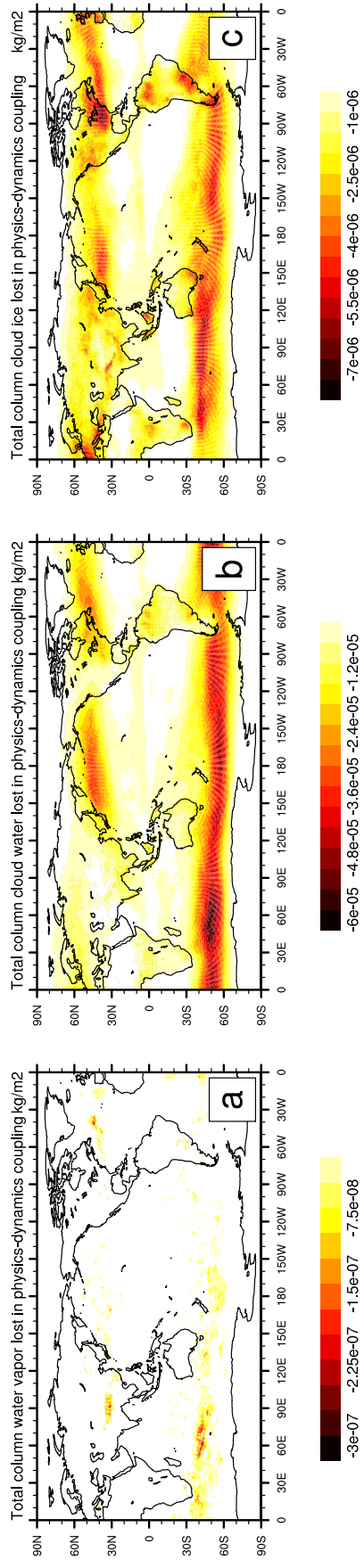


**Figure 6.** One year average of mass  $[kg/m^2]$  'clipped' in physics-dynamics coupling (so that state is not driven negative) when using `ftype=0` ('dribbling') physics-dynamics coupling for (a) water vapor, (b) cloud liquid and (c) cloud ice, respectively. Interestingly the element boundaries systematically show in the plots which is likely related to the anisotropy of the quadrature grid [Herrington *et al.*, 2018].

## TE tendencies for the default CAM-SE configuration (AMIP)

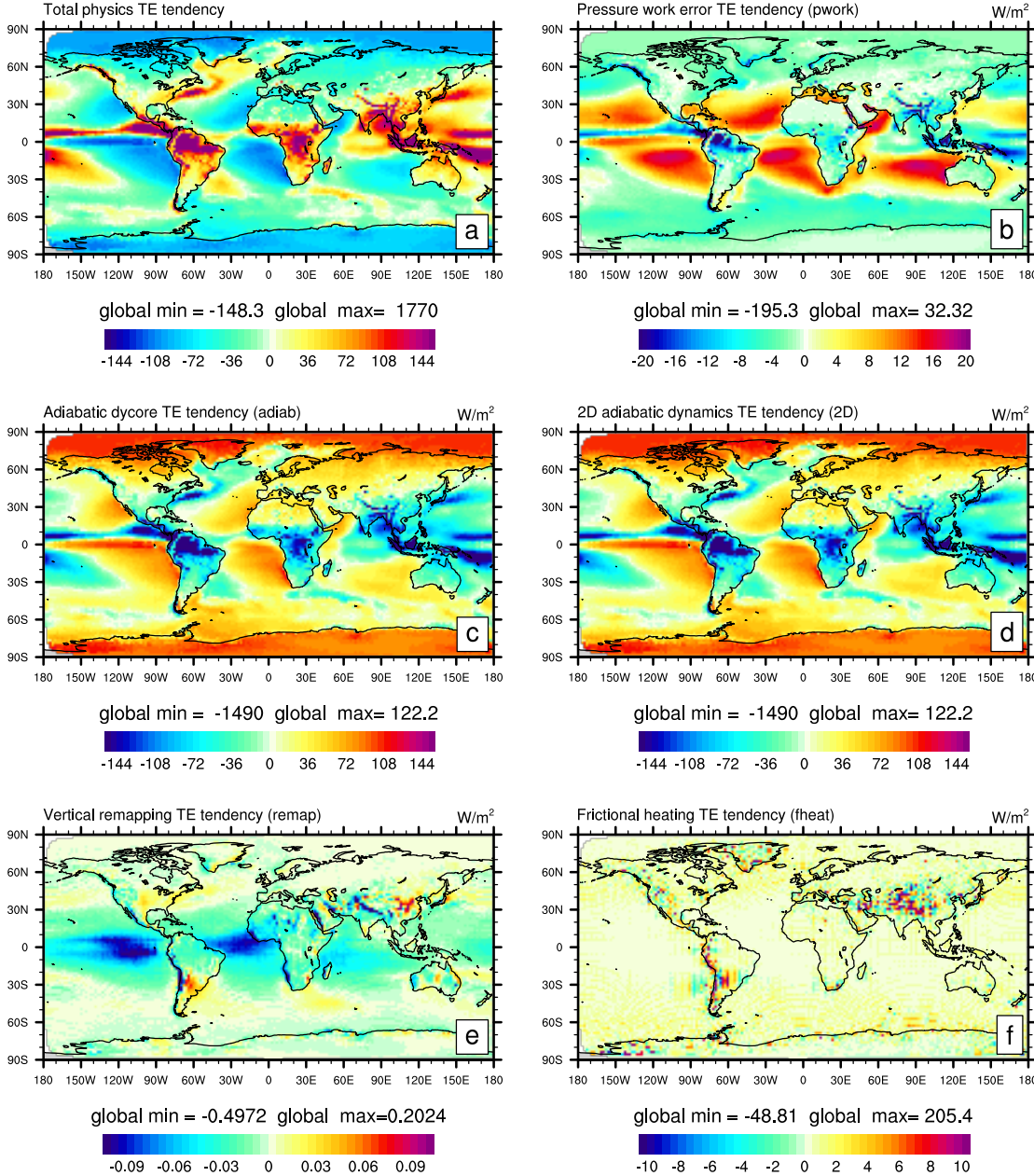


**Figure 7.** Two-dimensional spatial structure of column-integrated TE tendencies for different terms in the TE tendency budget using the *default* configuration: Column-integrated (a)  $\partial E^{(param)}$ , (b)  $\partial E^{(pwork)}$ , (c)  $\partial E^{(adiab)}$ , (d)  $\partial E^{(2D)}$ , (e)  $\partial E^{(remap)}$ , and (f)  $\partial E^{(fheat)}$ . Above each color bar the global minimum and maximum TE tendencies are noted as there are small number of grid points where the TE tendencies are much larger than the color bar range.